Supplementary Information

Table of Contents

Other Supplementary Materials for this manuscript include the following:

Supplementary Movies S1 to S10

I. Experimental details

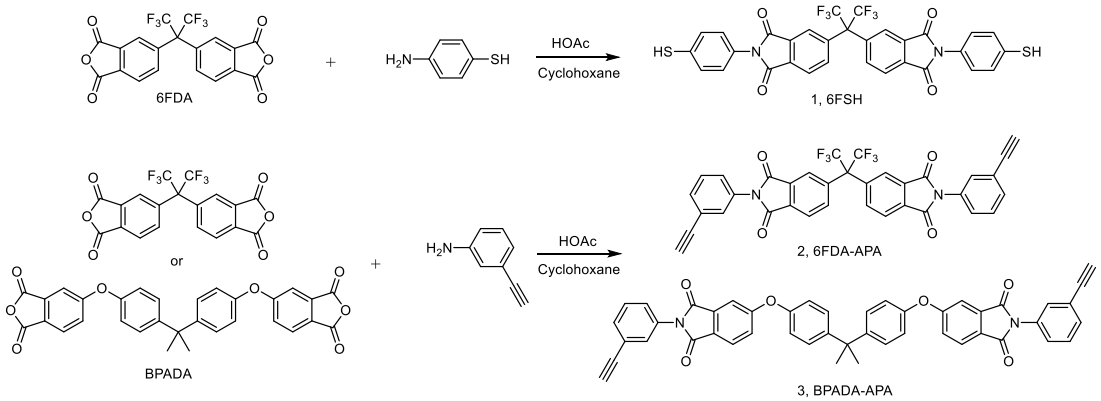

Supplementary Fig. 1. Synthesis of monomer 1-3.

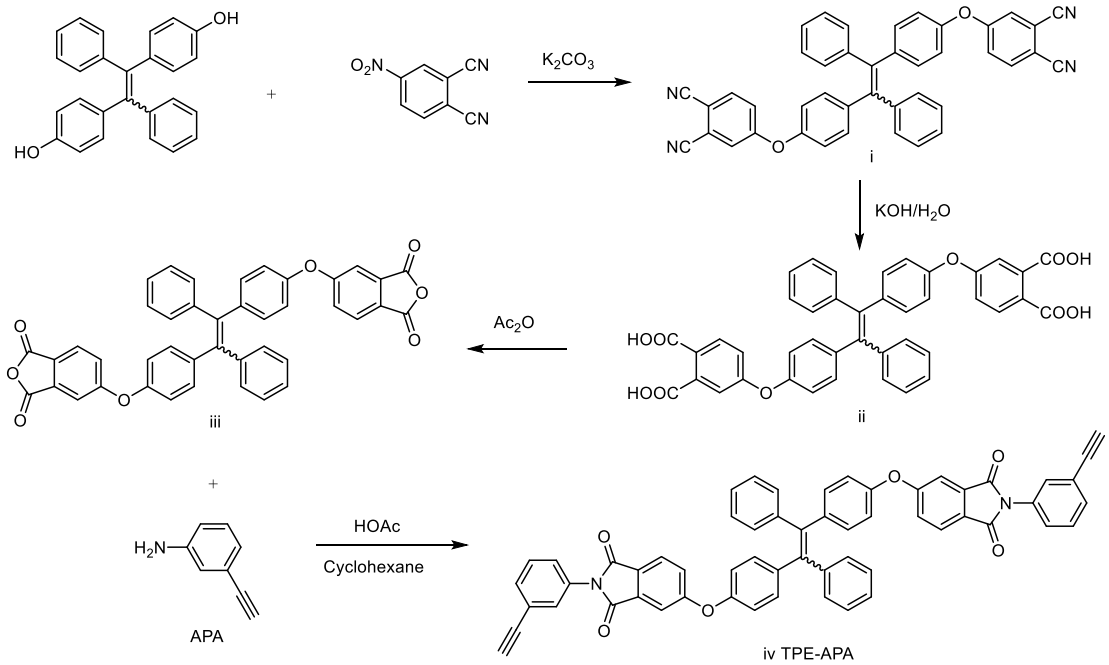

Supplementary Fig. 2. Synthesis of monomer 4 TPE-APA.

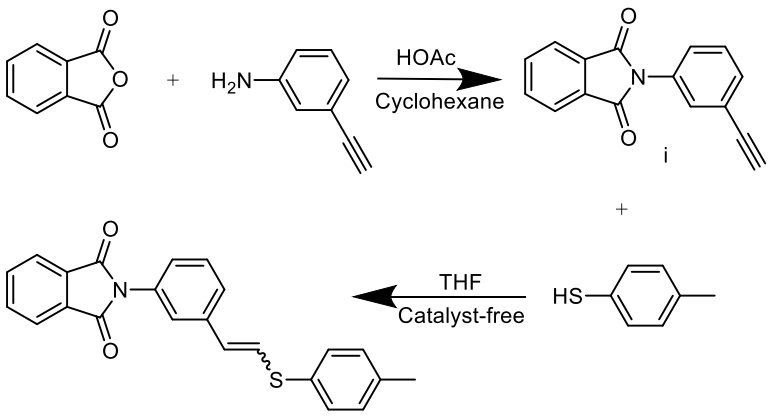

Supplementary Fig. 3. Synthesis of model compound.

II. Investigation of reaction conditions

We first studied the effect of temperature on the polymerization using **1** and **2** as reactants. It was found that the thiol-yne click polymerization performed at 30 °C could produce PIs with highest molecular weight in 15 min (Supplementary Table 1, Entry 1-3). When the temperature was raised to 40 °C, the molecular weight of 6FDA-PI slightly decreased. All in all, 30 °C was finally awarded the optimal reaction temperature. Based on the above optimization temperature, we focused on the time course of the polymerization. The results showed that the polymerization of **1** and **2** is so efficient that the viscosity increased rapidly in just a few minutes and a polymer with M_w of 94 kDa was yielded even after as short as 10 min (Supplementary Table 1, Entry 5), which is much more efficient than those with other catalyzed systems. Further prolonging the reaction time exerted a little effect on the M_w, so the reaction time was eventually set as 15 min. Besides, the effect of monomer concentration on the M_w was also investigated. The fact that the highest M_w was obtained when the monomer concentration was 0.15 M made us choose this concentration for subsequent polymerization (Supplementary Table 1, Entry 7-9). Under optimal conditions, the other two PIs could also be prepared smoothly (Supplementary Table 2, Entry 4, 5). Then we explored polymerization in the dark and in the air (Supplementary Table 2, Entry 2, 3). The results showed that the reaction could proceed smoothly in the dark but not in air. Then we investigated the polymerization mechanism. In general, the thiol-yne reactions, considered as a sister reaction to the well-known thiol-ene reaction, can follow a radical- or nucleophile-dominated mechanism. The polymerization of **1** and **2** couldn't produce high M_w polymer in the presence of γ-terpinene, a well-known radical trapper, suggesting the radical-mediated mechanism of this catalyst-free thiol-yne polymerization (Supplementary Table 2, Entry 6). As for the source of free radicals, presumably, it is the result of aromatic disulfide exchange. It is well-known that the dithiols can be easily oxidized to disulfide bonds[1]. Previous studies have demonstrated that aromatic disulfide bonds can exchange without any stimulus at room temperature[2,3], during which sulfur radicals can be produced and then attack the electron-rich triple bonds. Consequently, this thiol-yne polymerization does not require any photo/thermal initiator, which will greatly simplify the operation and reduce experimental requirements.

The structures of the PIs have been characterized by FT-IR and ^{1}H-NMR spectroscopy. Supplementary Fig 15 and Supplementary Fig 18 show the representative spectra of 6FDA-PI and its monomers 1 and 2. The characteristic absorption bands at 2551 and 3285 cm^{-1} corresponding to the stretching vibrations of S−H and ≡C−H in 1 and 2 respectively disappear in the FT-IR spectrum of the 6FDA-PI polymer, suggesting the completion of the polymerization reaction. Meanwhile, the FT-IR spectrum of 6FDA-PI shows the characteristic absorption bands of the asymmetric and symmetric vibrations of imide carbonyl groups at ca. 1783 cm^{-1} and 1723 cm^{-1}, respectively, and a C–N–C stretching vibration band at ca. 1372 cm^{-1}, indicating the incorporation of five-membered imide ring to the polymer backbone. The ^{1}H-NMR spectrum showed that the mercapto and ethynyl protons of 1 and 2 respectively resonating at 3.56 ppm

and 3.14 ppm are almost or completely disappeared in the spectrum of 6FDA-PI polymer, further conforming the high conversion of diyne and dithiol. Similar results are also achieved for BPADA-PI and TPE-PI (Supplementary Figs. 16−20). Meanwhile, the new peaks of protons corresponding to vinylene sulfide were clearly observed between δ 6.97-6.58 in the ^{1}H NMR spectrum of 6FDA-PI. Because of the large difference in chemical shifts of the stereoisomers, the *E*- and *Z*-vinylene protons can be recognized in the ^{1}H NMR spectrum and their ratio is calculated using the integrals. The *E*/*Z* ratio of 6FDA-PI is estimated to be 37/63 (Supplementary Fig. 21), while 35/65 for BPADA-PI and 63/37 for TPE-PI, respectively. (Supplementary Figs. 22−23). Furthermore, all the polyimides show no resonances of double addition products. This is most likely the result of the low reactivity and significant steric hindrance of this kind of ethylene linkage, due to the conjugation of vinyl with benzene ring, which impedes its subsequent reactions.

Supplementary Table 1. Optimization of Polymerization Reaction of 1 and 2

entry[a]	[M][b] (M)	*T* (°C)	time (min)	M_w[b]	M_w/M_n[b]	yield (%)
Screening of temperature						
1	0.15	25	15	65295	2.05	89
2	0.15	30	15	108756	2.68	93
3	0.15	40	15	72696	2.17	90
Screening of reaction time						
4	0.15	30	5	44255	2.17	78
5	0.15	30	10	94030	2.45	93
6	0.15	30	15	108756	2.68	93
Screening of monomer concentration						
7	0.10	30	15	49063	1.86	82
8	0.15	30	15	108756	2.68	93
9	0.20	30	15	62259	2.04	94

[a]Carried out in THF under argon. [b] Estimated by gel-permeation chromatography (GPC) in THF on the basis of a polystyrene calibration. The data are in the unit of g·mol^{-1}; M_w = weight-average molecular weight; M_w/M_n = polydispersity index (PDI); M_n = number-average molecular weight.

Supplementary Table 2. Click Polymerization of Dithiol 1 with Diynes 2, 3 and 4

Entry[a]	Monomers	Polymers	Yield (%)	M_w[b]	PDI[b]	E/Z[c]
1	1+2	6FDA-PI	93	108756	2.68	37/63
2[d]	1+2	6FDA-PI	91	81598	2.64	
3[e]	1+2	6FDA-PI	42	13246	1.51	
4	1+3	BPADA-PI	90	126231	2.48	35/65
5	1+5	TPE-PI	91	67530	2.30	63/37
6[f]	1+2	6FDA-PI	36	9782	1.24	

[a]Carried out in THF at 30 °C under argon for 15 min, [M] = 0.15 M. [b]Estimated by gel-permeation chromatography (GPC) in THF on the basis of a polystyrene calibration. The data are in the unit of g·mol^{-1}; M_w = weight-average molecular weight; M_w/M_n = polydispersity index (PDI); M_n = number-average molecular weight. [c]Calculated from ^{1}H-NMR spectra. [d]Reacted in darkness. [e]Reacted in air. [f]Reacted in the presence of γ-terpinene (50 mM).

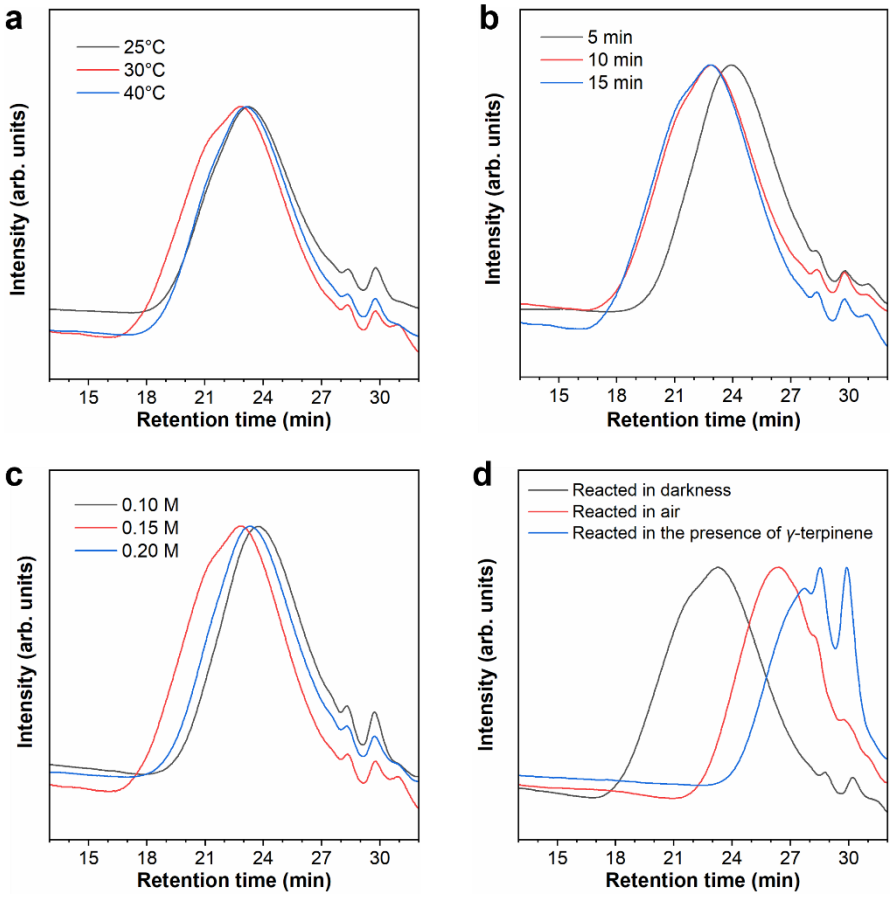

Supplementary Fig. 4. GPC curves of PIs. (a) Supplementary Table 1, entries 1–3; (b) Supplementary Table 1, entries 4-6; (c) Supplementary Table 1, entries 7-9 and (d) Supplementary Table 2, entries 2, 3 and 6.

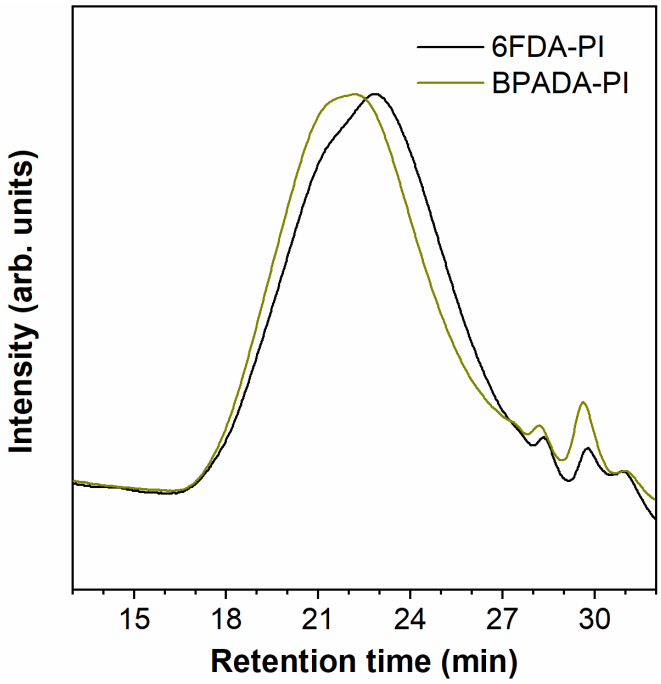

Supplementary Fig. 5. GPC curves of the polymers 6FDA-PI and BPADA-PI.

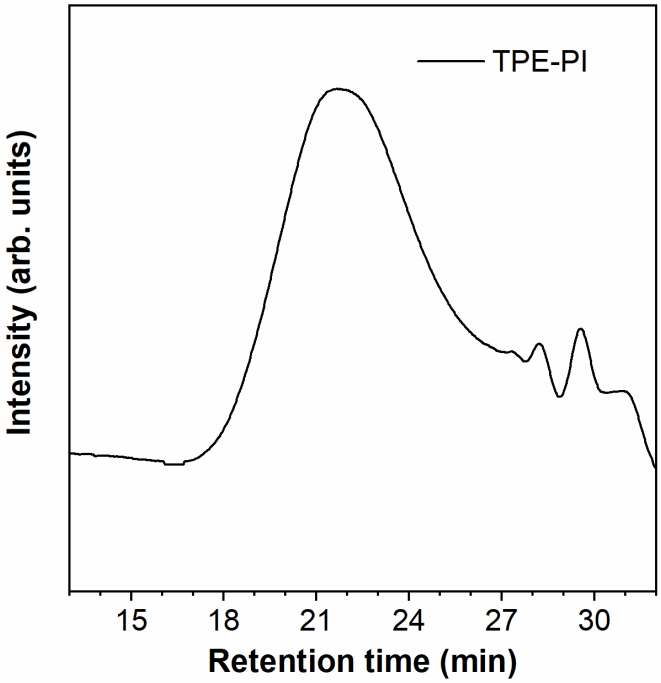

Supplementary Fig. 6. GPC curves of the polymer TPE-PI.

III. Additional Characterizations

Supplementary Table 3. Solubility of the PIs[a]

Polyimide	NMP	m-Cresol	DMAc	DMF	THF	$CHCl_3$	DCM
6FDA-PI	+ +	+ +	+ +	+ +	+ +	+ +	+ +
BPADA-PI	+ +	+ +	+ +	+ +	+ +	+ +	+ +
TPE-PI	+ +	+ +	+ +	+ +	+ +	+ +	+ +

[a]+ +: Soluble at room temperature; + -: Partially soluble; - -: Insoluble; NMP: N-methylpyrrolidone, DMAc: N,N-dimethylacetamide, DMF: N,N-dimethylformamide, THF: tetrahydrofuran, $CHCl_3$: trichloromethane, DCM: dichloromethane.

Supplementary Table 4. Mechanical and Thermal Properties of the PIs

Polyimide	T_S[a] (MPa)	T_M[b] (GPa)	E_b[c] (%)	Toughness[d] (MJ/m^3)	T_g[e] (°C)	$T_{d5\%}$[f] (°C)	$T_{d10\%}$[f] (°C)	$Rw\%$[g]
6FDA-PI	115.3±1.1	2.37±0.03	8.4±0.3	6.37±0.35	265	482	523	57.2
BPADA-PI	116.2±1.4	2.61±0.09	7.2±0.7	5.26±0.67	235	469	500	58.0
TPE-PI	94.1±1.4	2.12±0.13	8.3±0.9	5.24±0.91	239	452	528	41.4

[a]Ultimate tensile strength. [b]Young's modulus. [c]Elongation at break. [d]The toughness was determined by dividing the area under the stress-strain curves. [e]Glass transition temperature determined by DMA. [f]Temperature at 5% and 10% weight loss, respectively. [g]Residual weight retentions at 800 °C.

Supplementary Table 5. Optical properties of the PI films

Polyimide	λ_{cutoff}[a] [nm]	T_{450}[b] [%]	n_{589}[c]	n_{1550}[c]	ν_D[d]	ν_D'[d]	D[e]	D'[e]
6FDA-PI	374	77.2	1.6535	1.6172	24.9427	101.5	0.0401	0.0099
TPE-PI	350	95.4	1.6806	1.6382	18.4444	64.2	0.0542	0.0156
BPADA-PI	371	77.5	1.7095	1.6705	19.8184	81.2	0.0505	0.0123
UV-10 min[f]	/	/	1.6805	1.6440	19.5546	104.2	0.0511	0.0096
UV-20 min[f]	/	/	1.6577	1.6191	24.9129	50.8	0.0401	0.0197
UV-30 min[f]	/	/	1.6443	1.6053	25.5675	46.3	0.0391	0.0216
UV-40 min[f]	/	/	1.6333	1.5957	26.1694	47.7	0.0382	0.0210

[a]Cutoff wavelength. [b]Transmittance at 450 nm (thickness ca. 10 μm). [c]Refractive index measured at 589.2 and 1550 nm. [d] ν_D = Abbé number = $(n_D - 1)/(n_F - n_C)$, where n_D, n_F, and n_C are the refractive index at wavelengths of Fraunhofer D, F, and C spectral lines of 589.2, 486.1, and 656.3 nm, respectively; ν_D' = modified Abbé number = $(n_{1319} - 1)/(n_{1064} - n_{1550})$, where n_{1319}, n_{1064}, and n_{1550} are the refractive index at 1319, 1064, and 1550 nm, respectively. The wavelengths of 1319 and 1064 nm are chosen due to the practical interest of a commercial laser wavelengths (Nd: YAG), The wavelength of 1550 nm is chosen due to its telecommunication importance. [e]D = chromatic dispersion in the visible region = $1/\nu_D$. D' = chromatic dispersion in the infrared region = $1/\nu_D'$.[f]**BPADA-PI** polymer after UV irradiation with 10, 20, 30, 40 min.

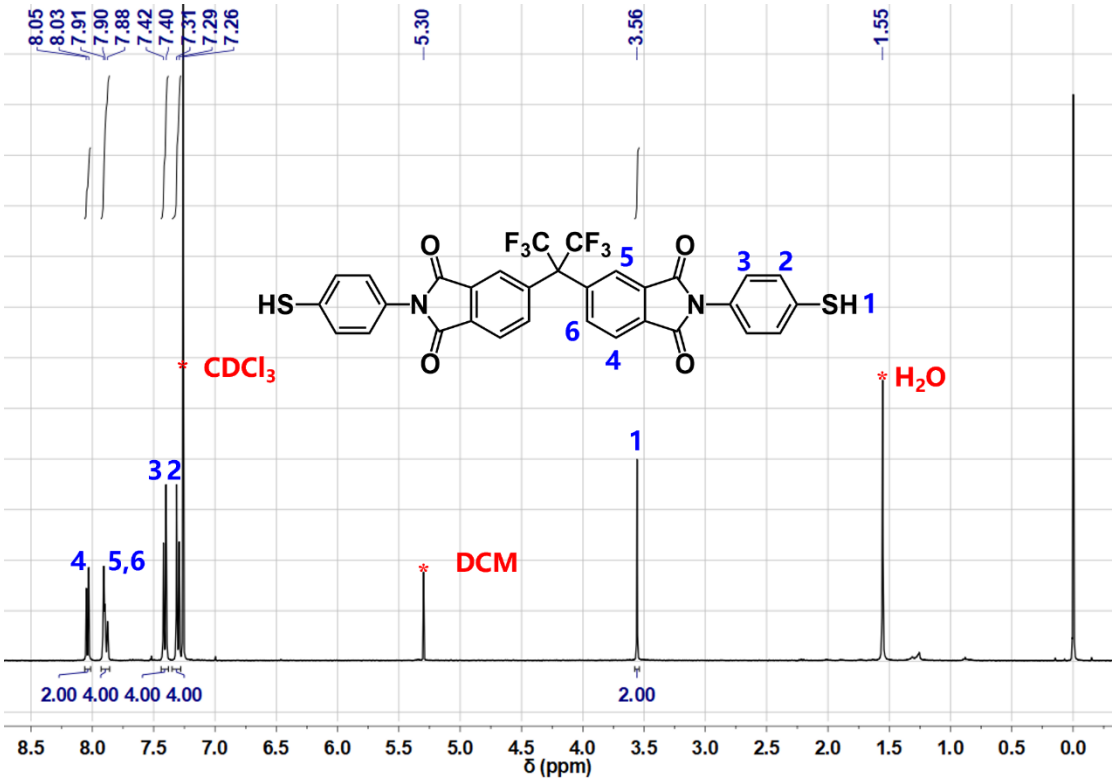

Supplementary Fig. 7. ^{1}H NMR spectrum of monomer 1 (6FSH) in $CDCl_3$. The solvent peaks are marked with asterisks.

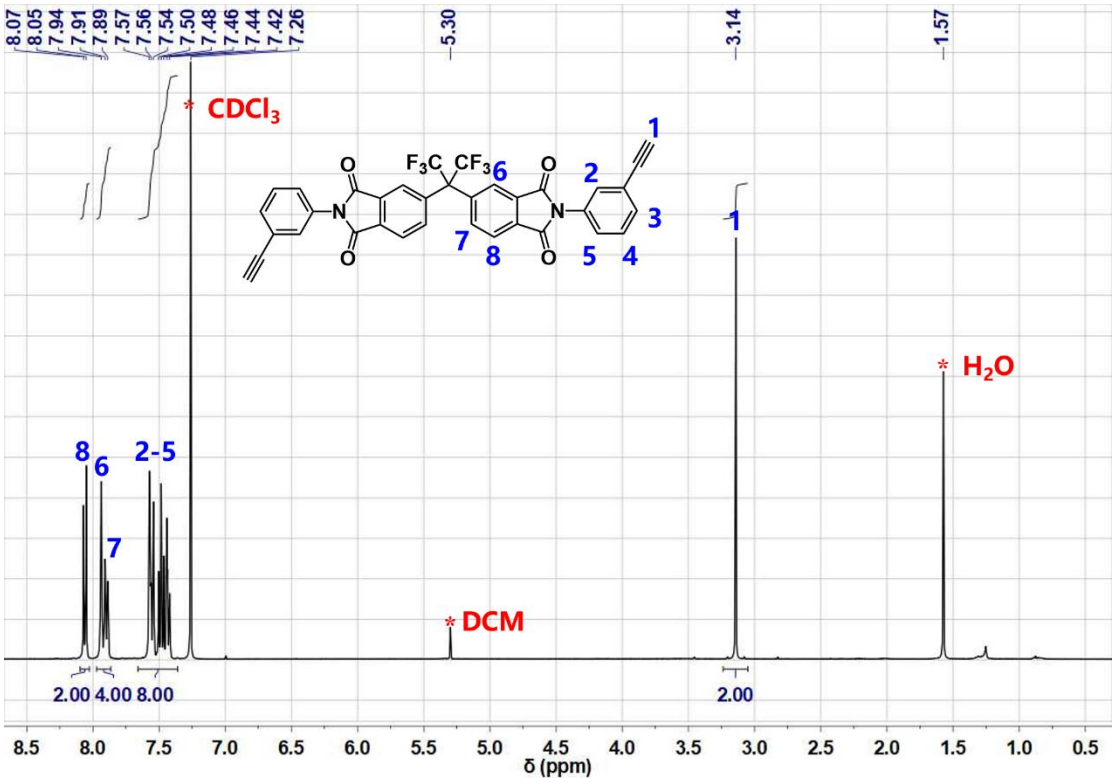

Supplementary Fig. 8. ^{1}H NMR spectrum of monomer 2 (6FDA-APA) in $CDCl_3$. The solvent peaks are marked with asterisks.

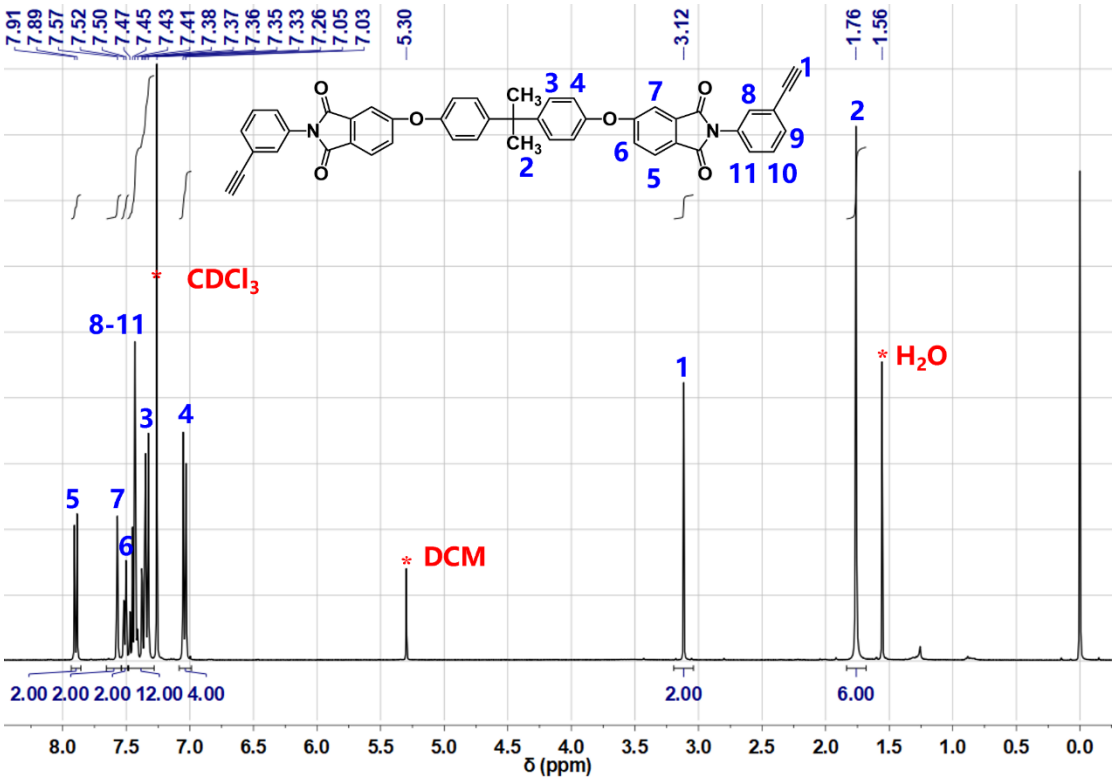

Supplementary Fig. 9. ^{1}H NMR spectrum of monomer 3 (BPADA-APA) in $CDCl_3$. The solvent peaks are marked with asterisks.

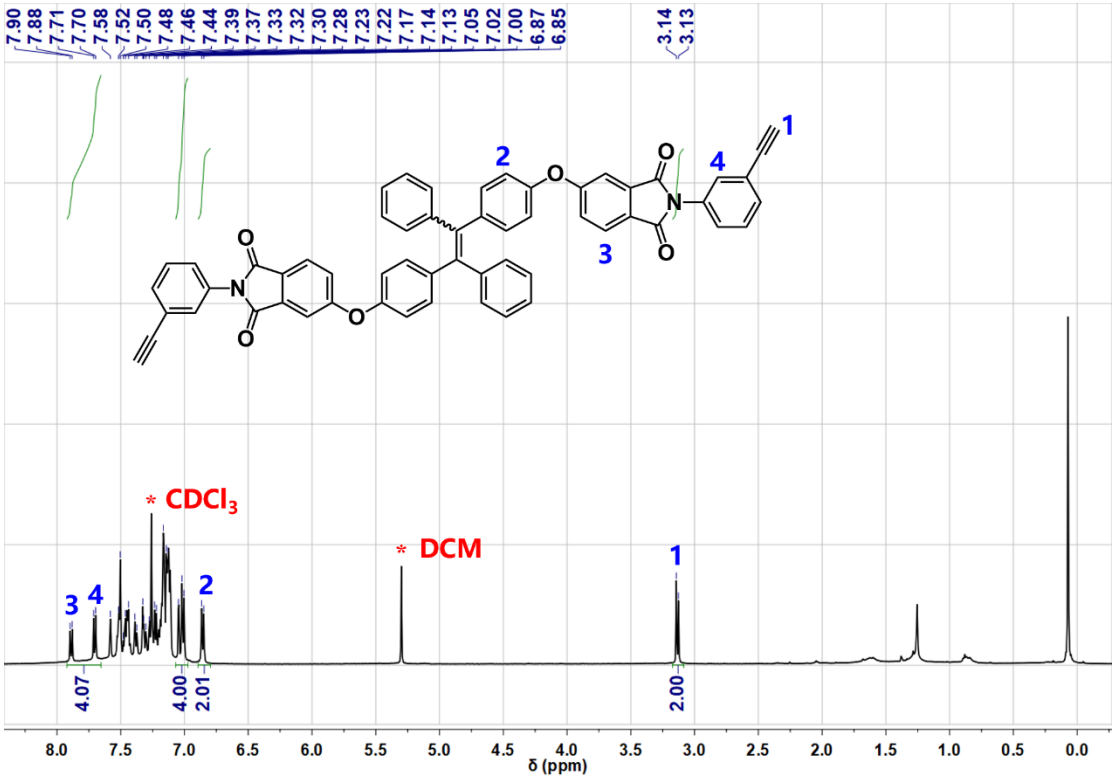

Supplementary Fig. 10. ^{1}H NMR spectrum of monomer 4 (TPE-APA) in $CDCl_3$. The solvent peaks are marked with asterisks.

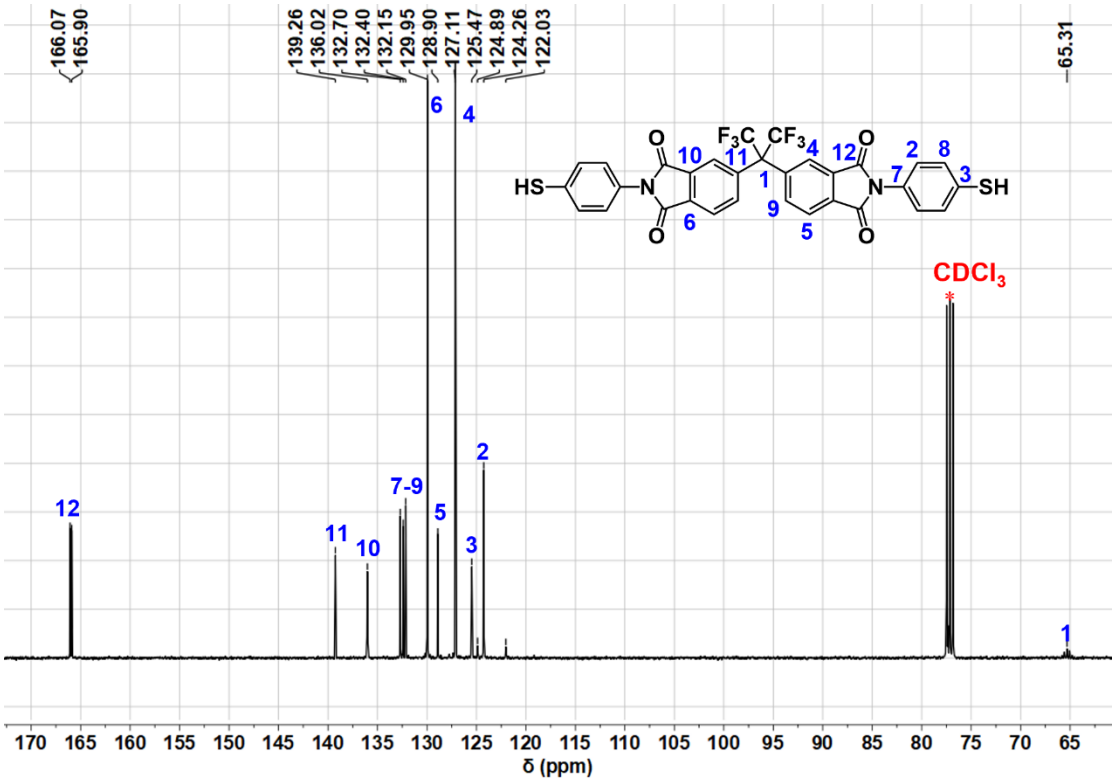

Supplementary Fig. 11. ^{13}C NMR spectrum of monomer 1 (6FSH) in $CDCl_3$. The solvent peaks are marked with asterisks.

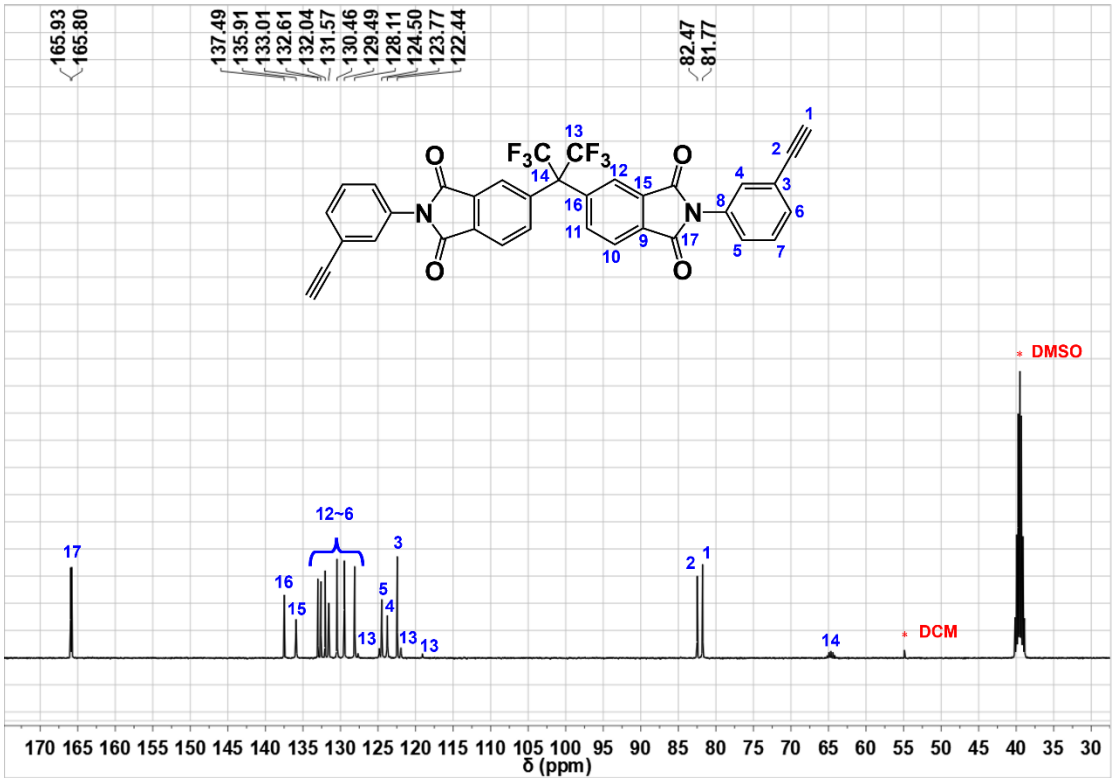

Supplementary Fig. 12. ^{13}C NMR spectrum of monomer 2 (6FDA-APA) in DMSO. The solvent peaks are marked with asterisks.

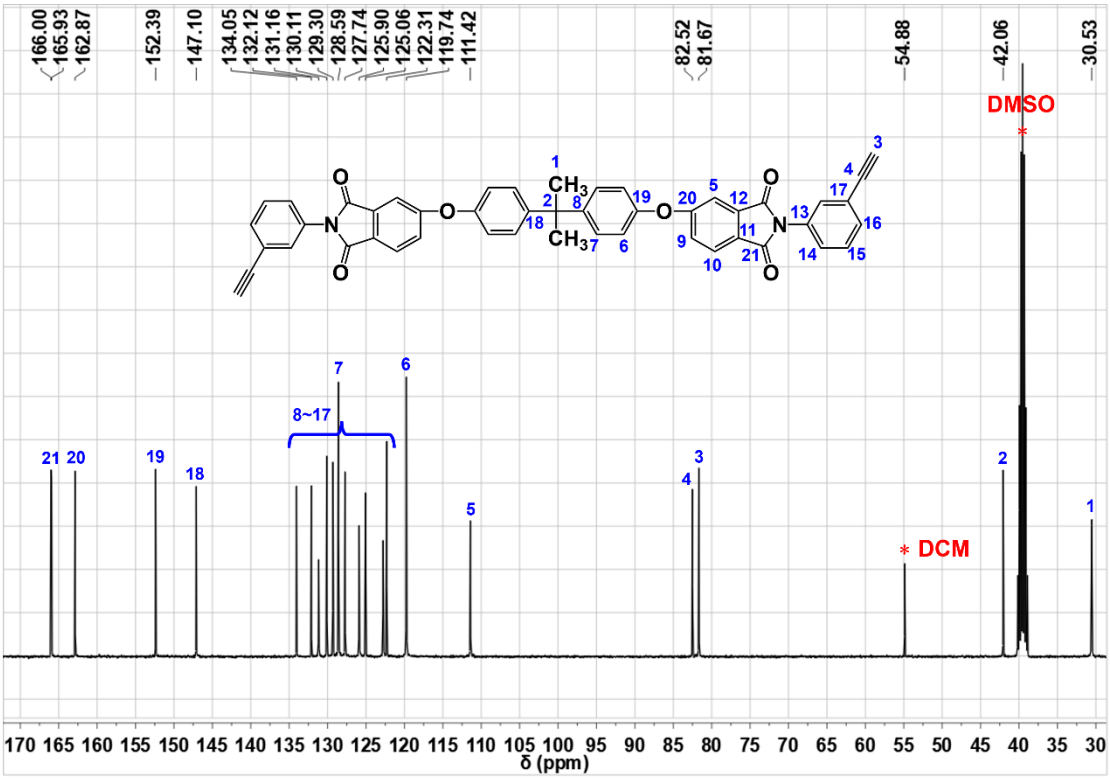

Supplementary Fig. 13. ^{13}C NMR spectrum of monomer 3 (BPADA-APA) in DMSO. The solvent peaks are marked with asterisks.

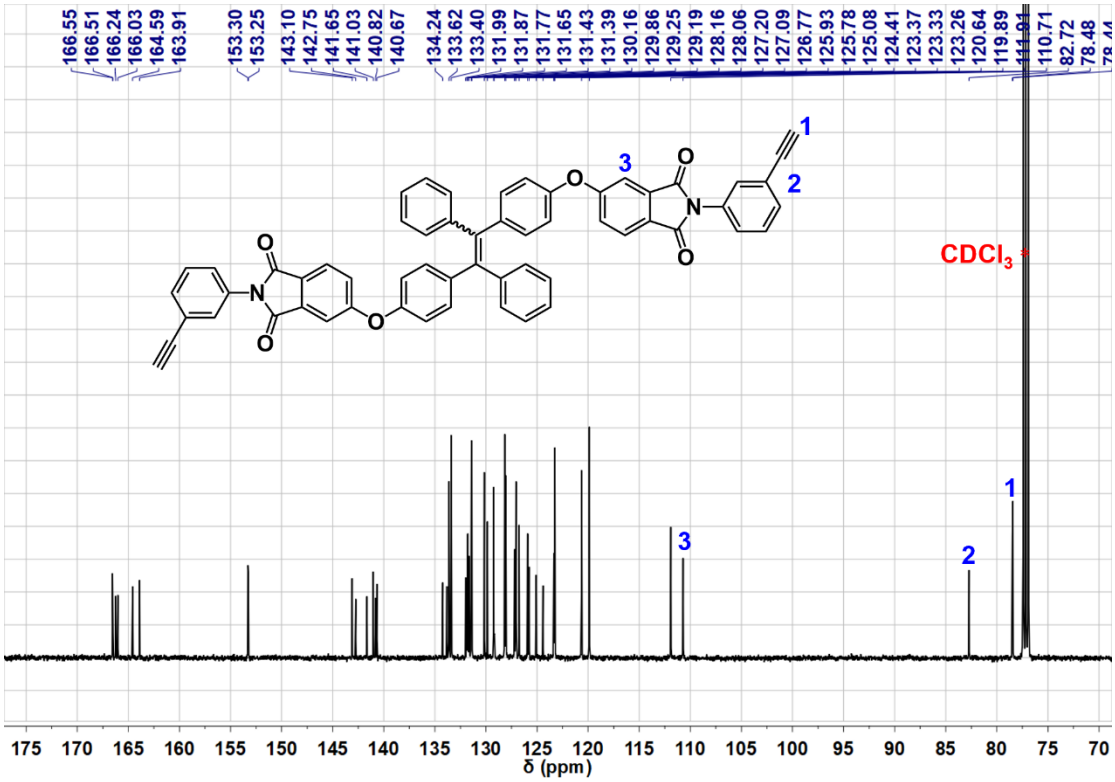

Supplementary Fig. 14. ^{13}C NMR spectrum of monomer 4 (TPE-APA) in $CDCl_3$. The solvent peaks are marked with asterisks.

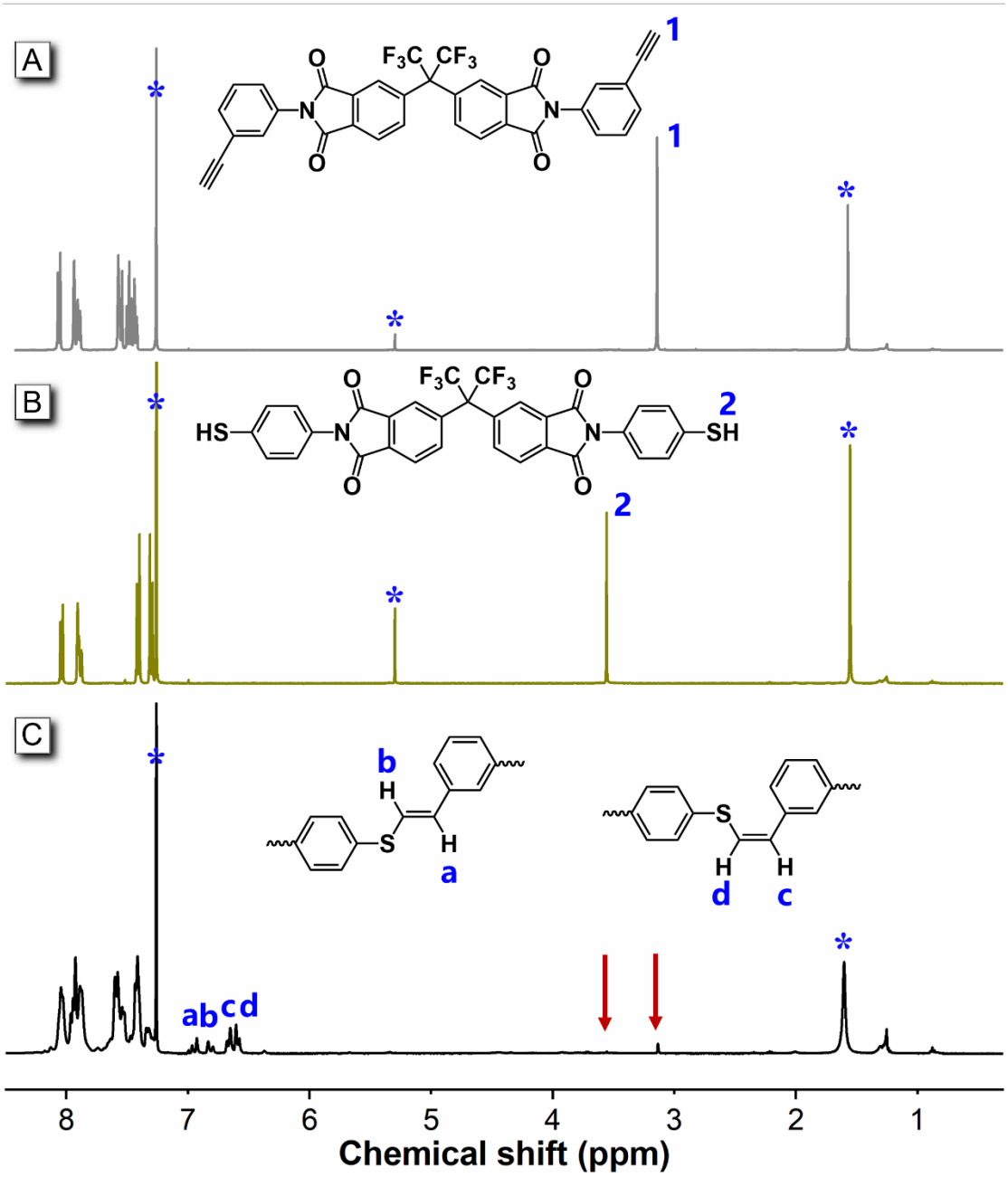

Supplementary Fig. 15. ^{1}H NMR spectra of monomers 2 (A), 1 (B), and 6FDA-PI (C) in $CDCl_3$.

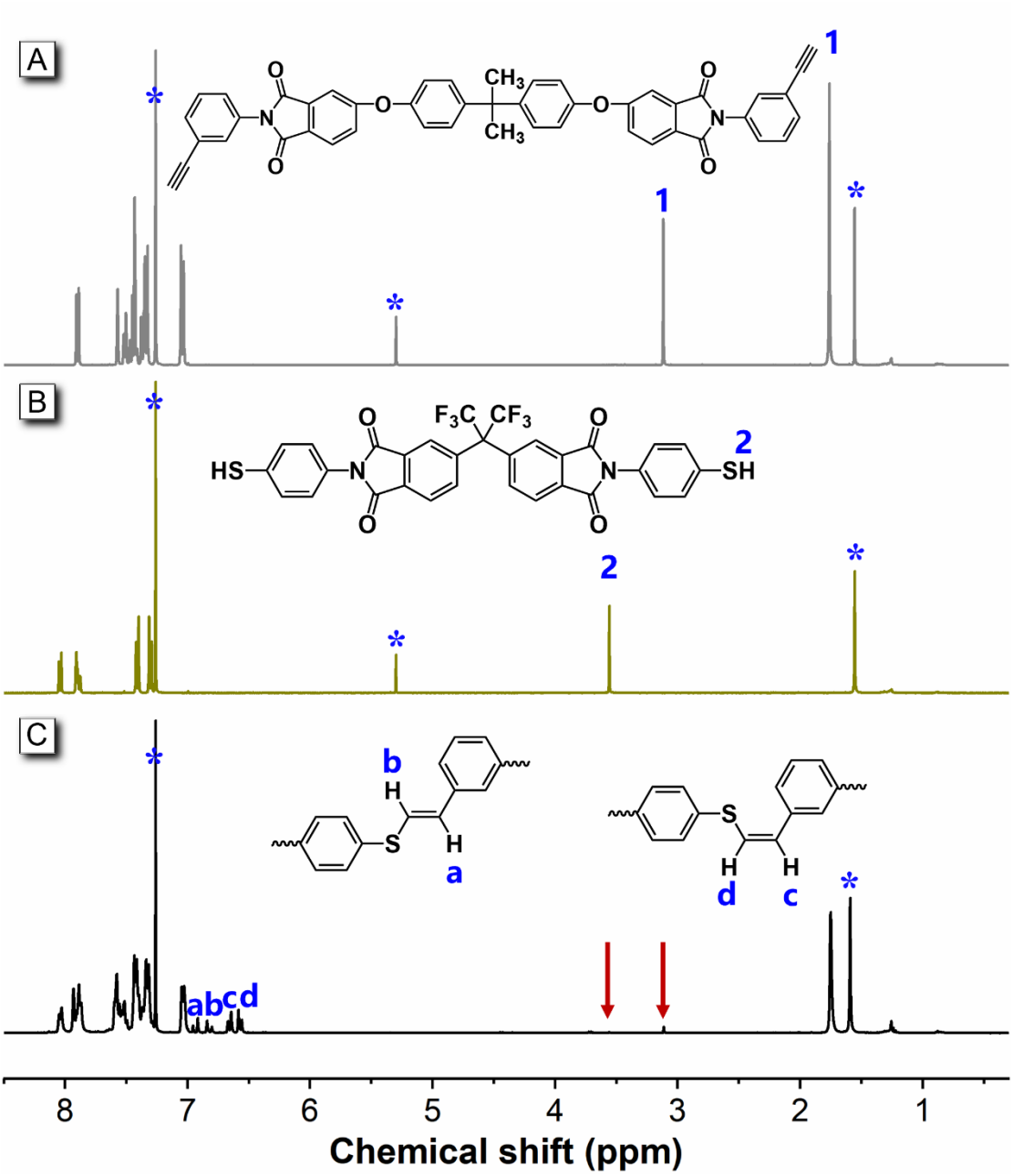

Supplementary Fig. 16. ^{1}H NMR spectra of monomers 3 (A), 1 (B), and BPADA-PI (C) in $CDCl_3$.

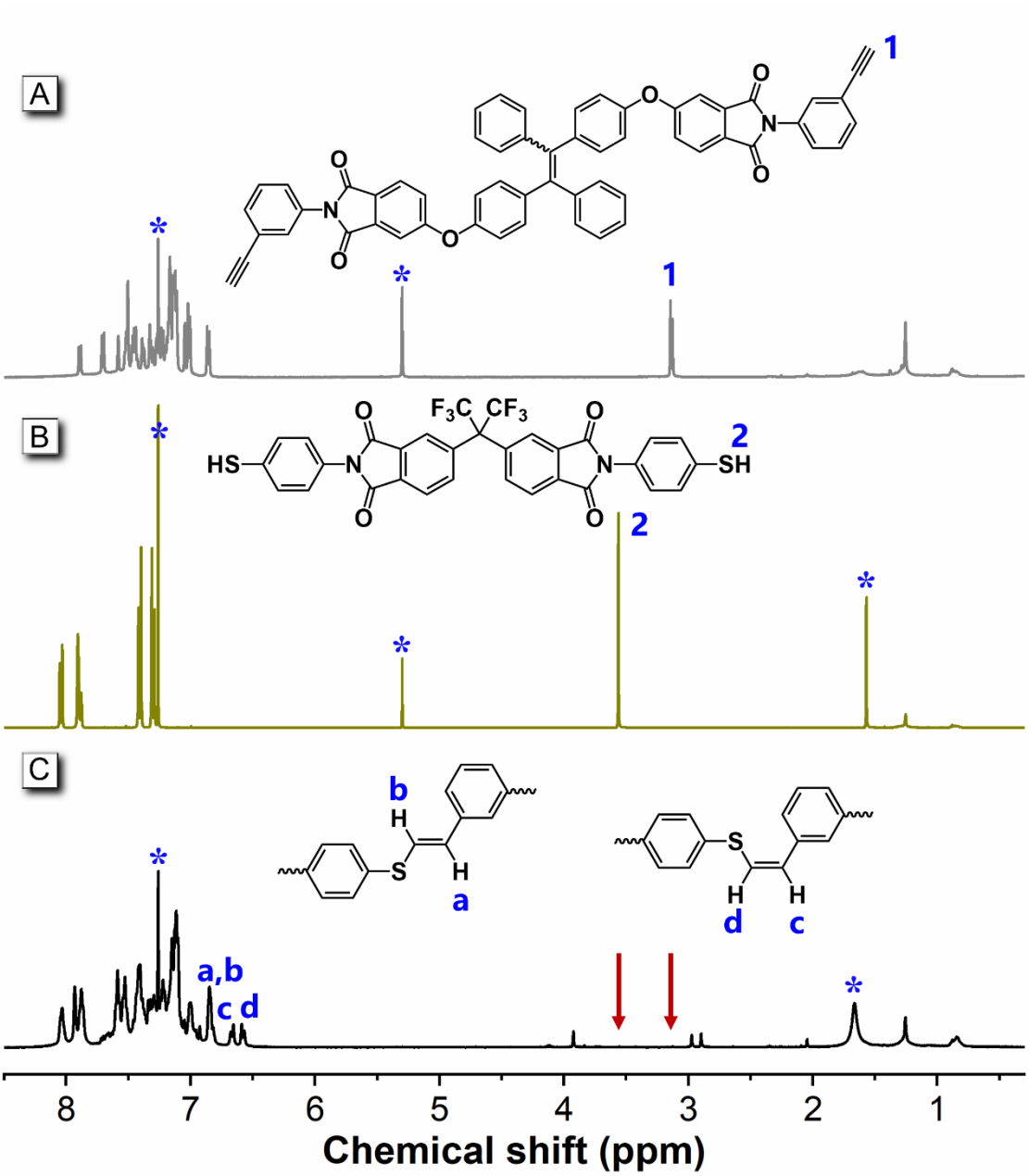

Supplementary Fig. 17. ^{1}H NMR spectra of monomers 4 (A), 1 (B), and TPE-PI (C) in $CDCl_3$.

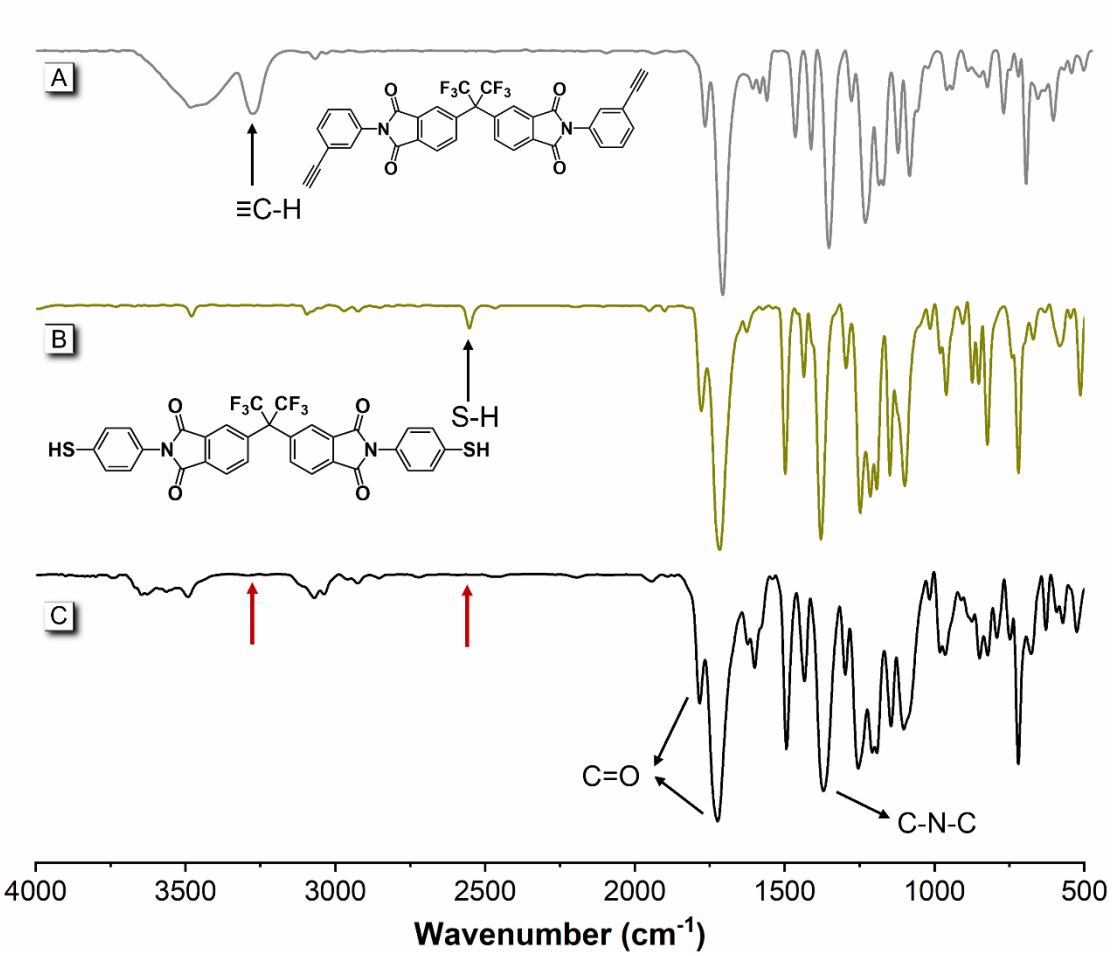

Supplementary Fig. 18. FT-IR spectra of monomers 2 (A), 1 (B), and 6FDA-PI (C).

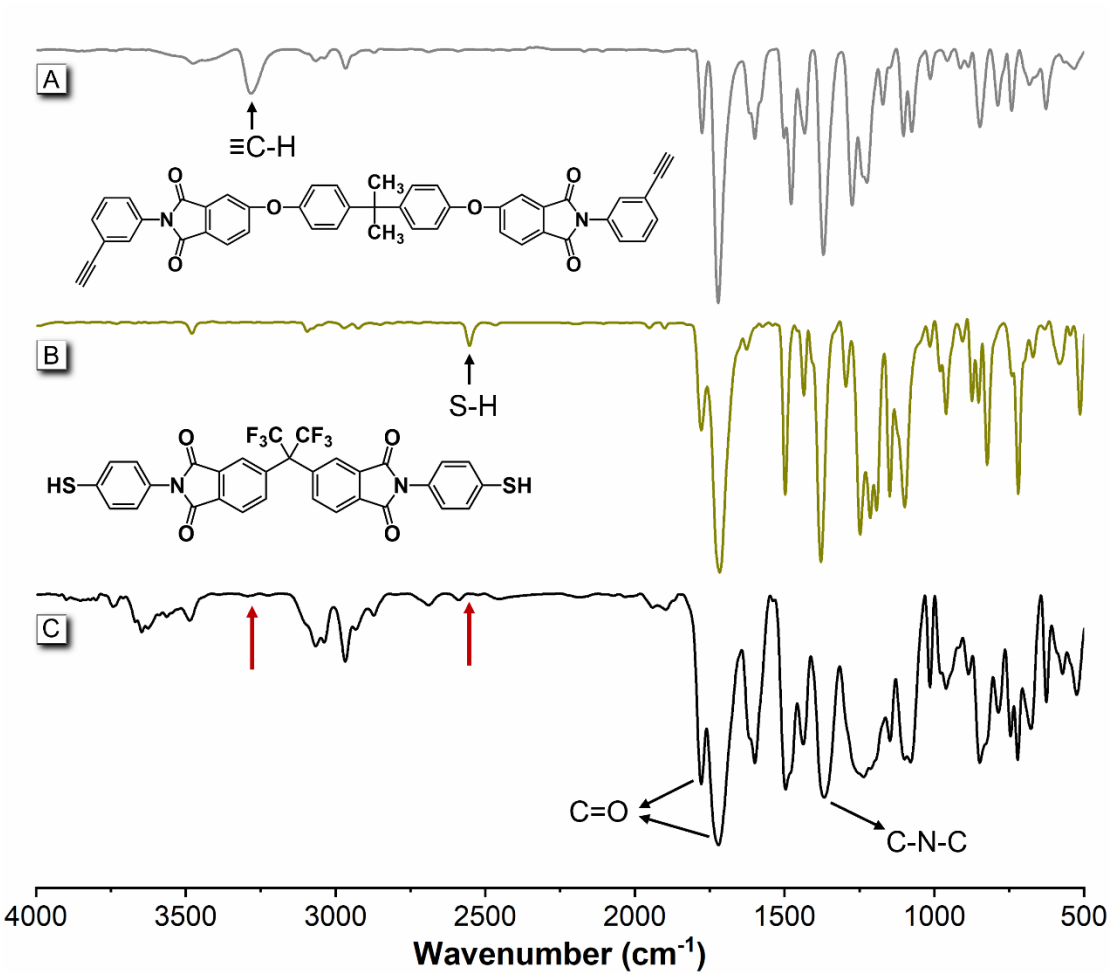

Supplementary Fig. 19. FT-IR spectra of monomers 3 (A), 1 (B), and BPADA-PI (C).

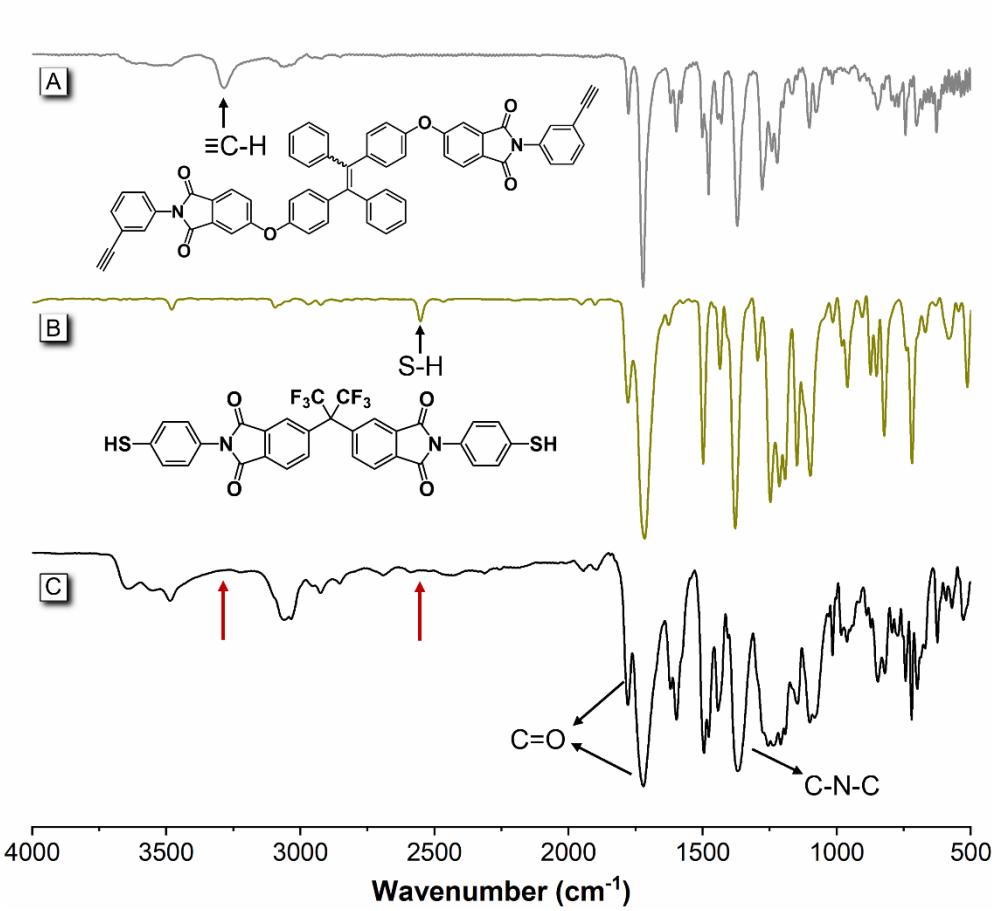

Supplementary Fig. 20. FT-IR spectra of monomers 4 (A), 1 (B), and TPE-PI (C).

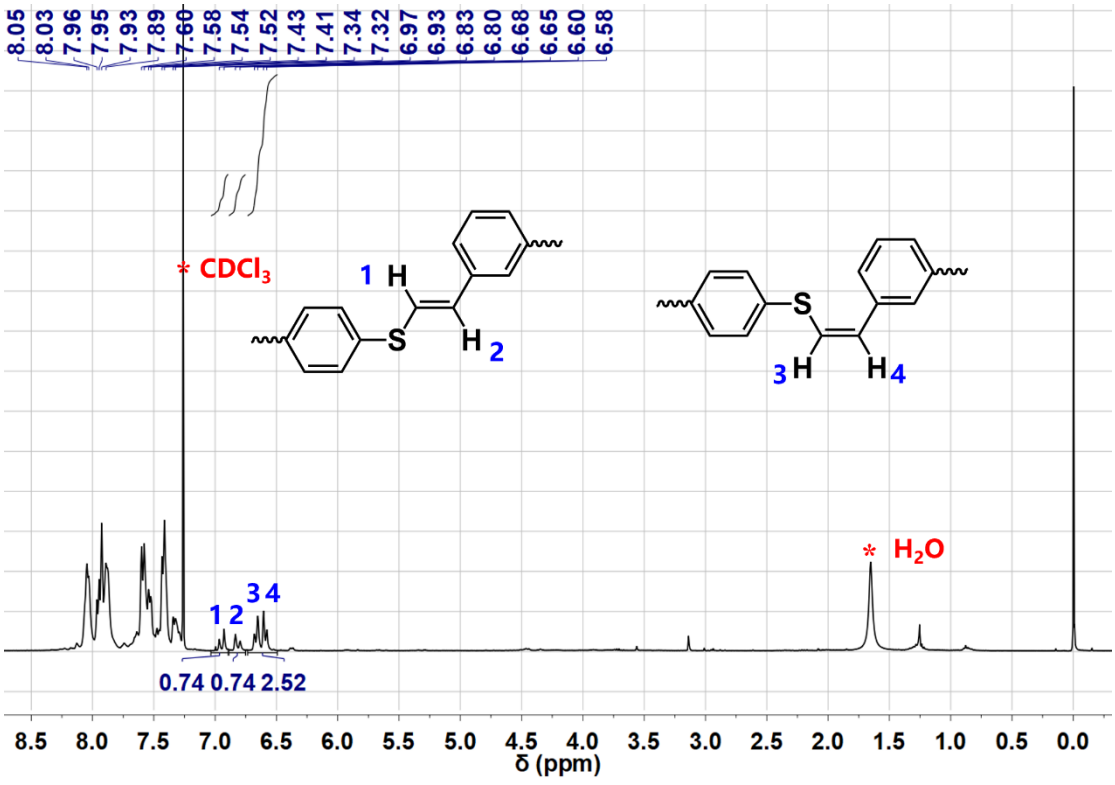

Supplementary Fig. 21. ^{1}H NMR spectrum of 6FDA-PI polymer in $CDCl_3$. The solvent peaks are marked with asterisks.

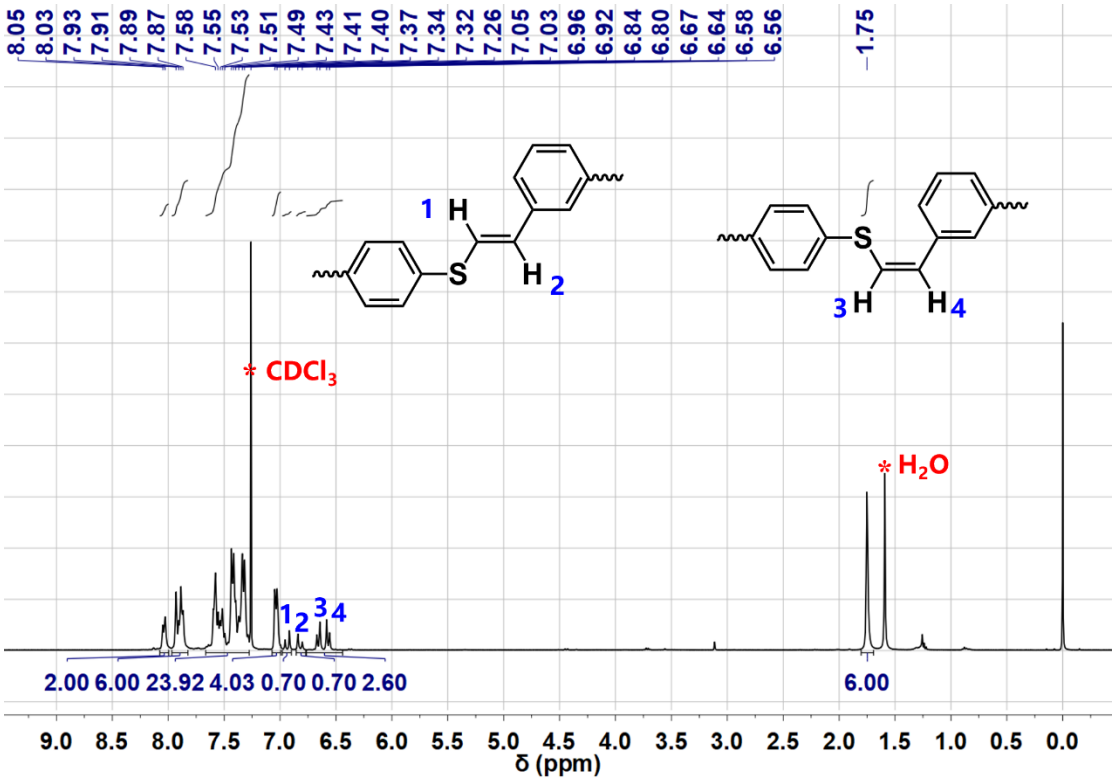

Supplementary Fig. 22. ^{1}H NMR spectrum of BPADA-PI polymer in $CDCl_3$. The solvent peaks are marked with asterisks.

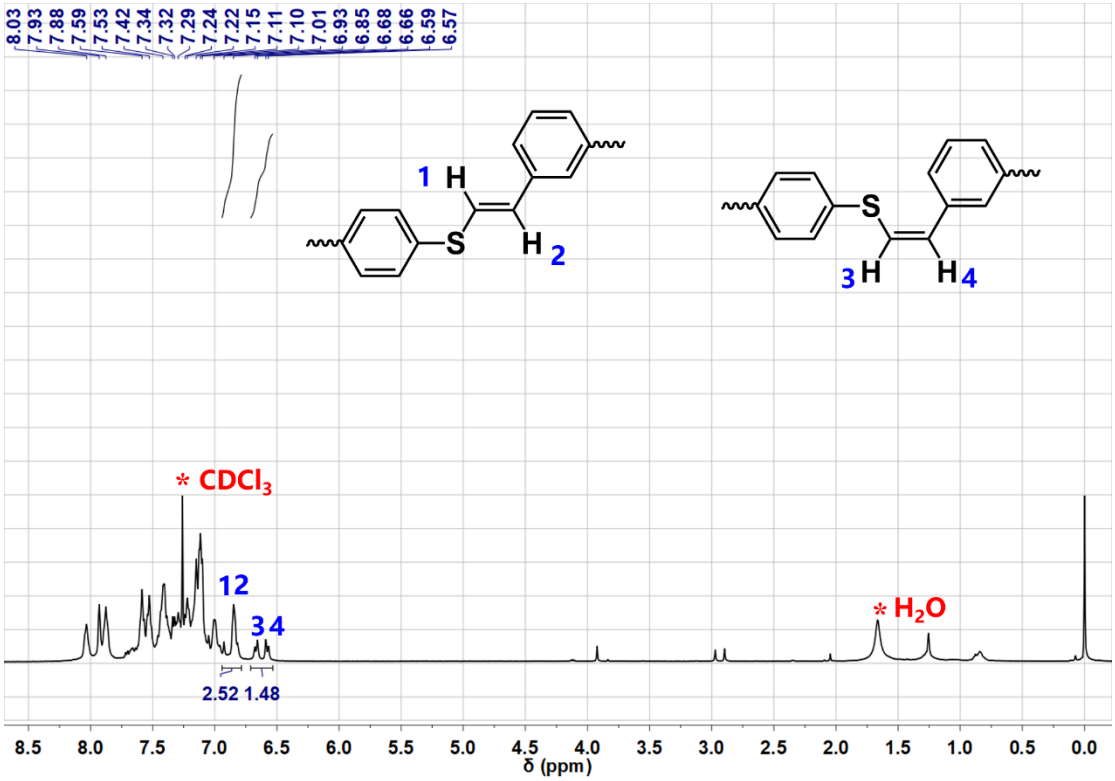

Supplementary Fig. 23. ^{1}H NMR spectrum of TPE-PI polymer in $CDCl_3$. The solvent peaks are marked with asterisks.

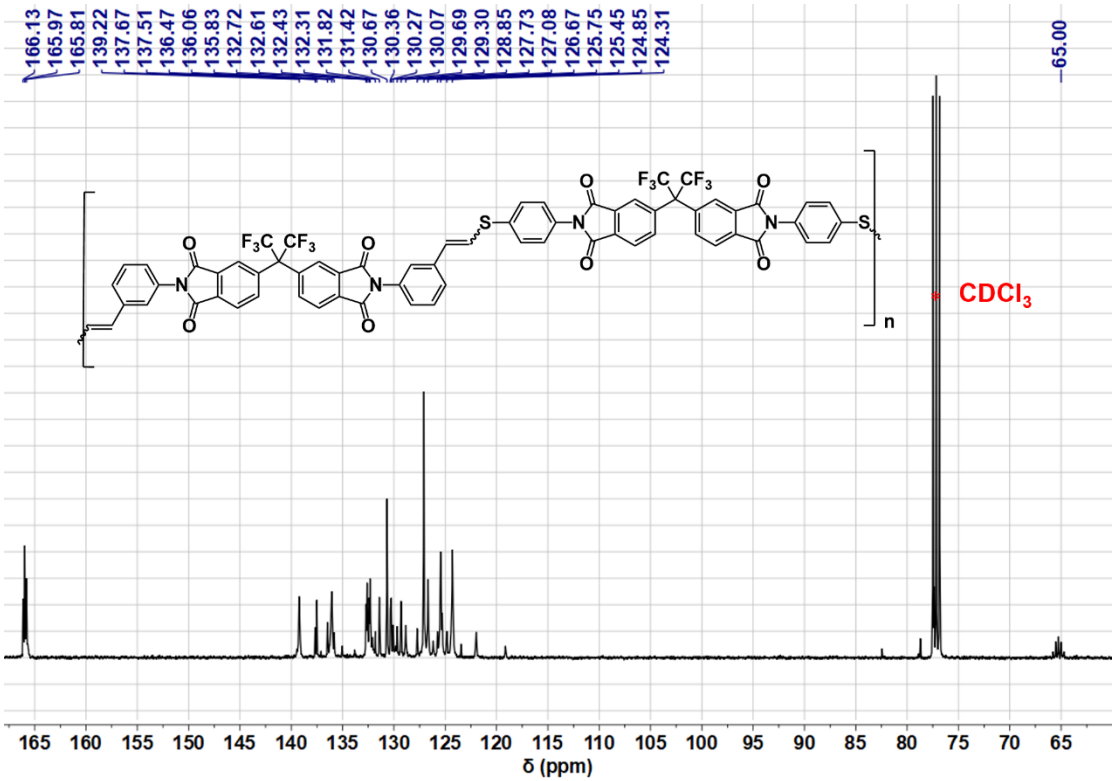

Supplementary Fig. 24. ^{13}C NMR spectrum of 6FDA-PI polymer in $CDCl_3$. The solvent peaks are marked with asterisks.

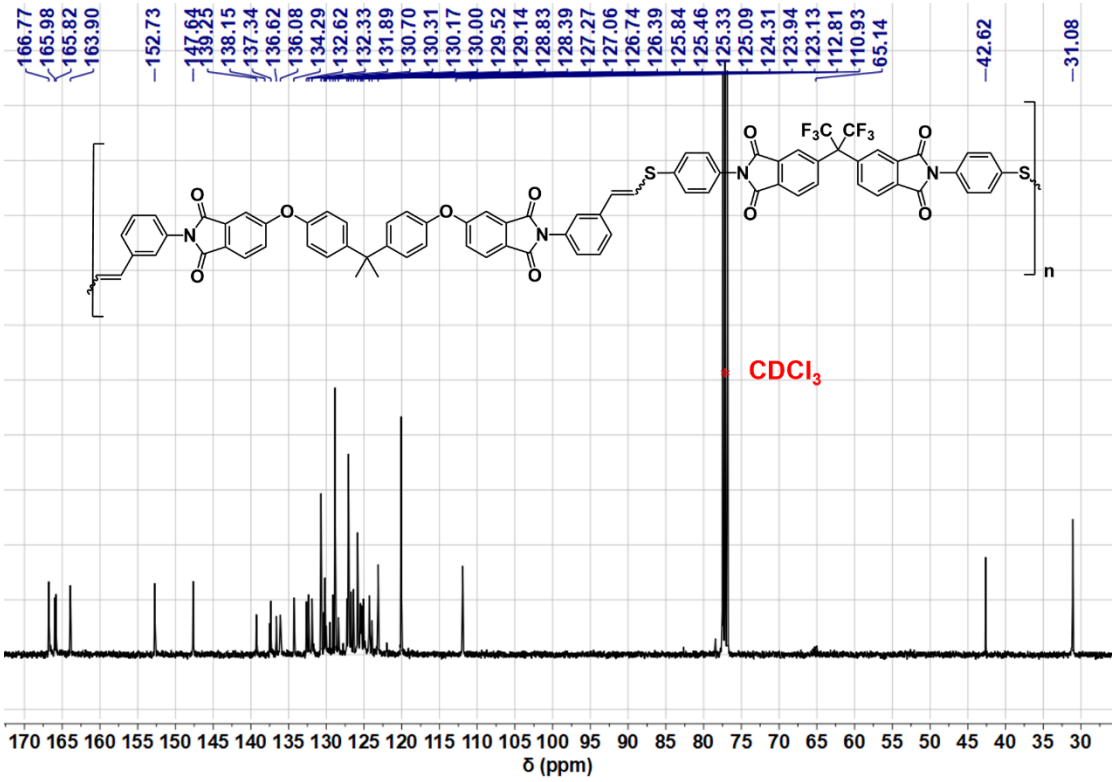

Supplementary Fig. 25. ^{13}C NMR spectrum of BPADA-PI polymer in $CDCl_3$. The solvent peaks are marked with asterisks.

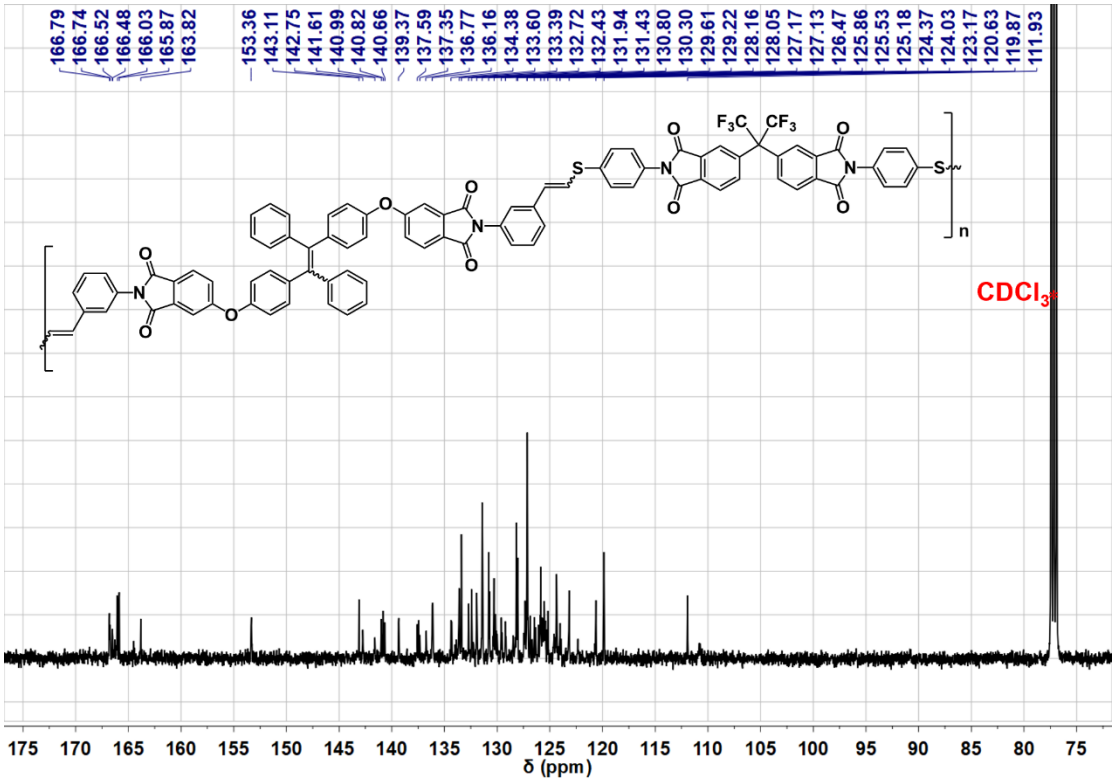

Supplementary Fig. 26. ^{13}C NMR spectrum of TPE-PI polymer in $CDCl_3$. The solvent peaks are marked with asterisks.

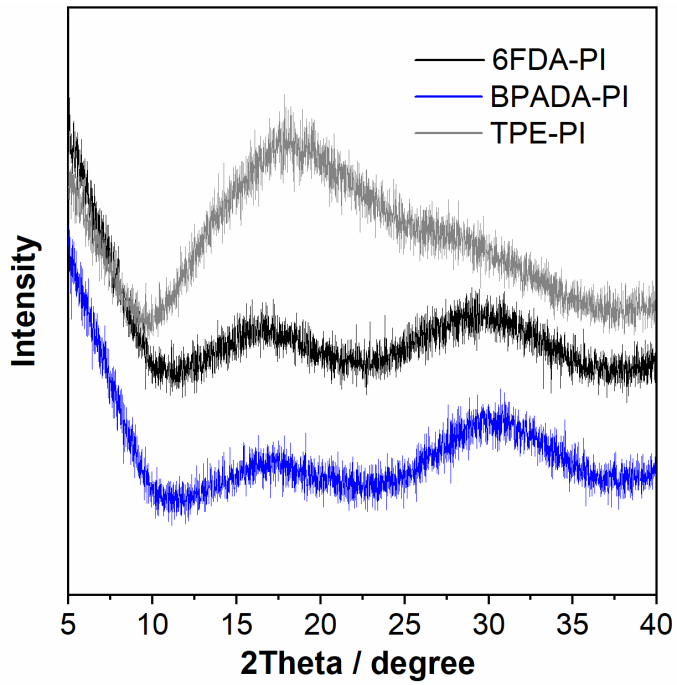

Supplementary Fig. 27. WAXD curves of PIs.

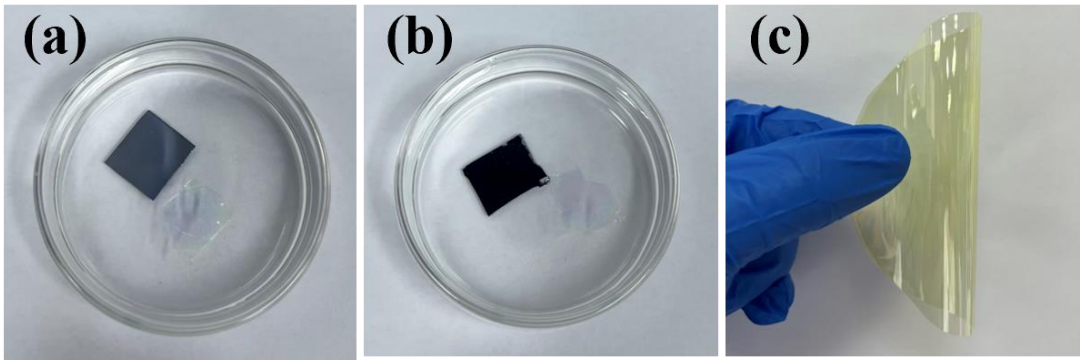

Supplementary Fig. 28. Optical graphs of PI films. (a) Optical graph of ultrathin freestanding film TPE-PI, 250 nm; (b) Optical graph of ultrathin freestanding film 6FDA-PI, 280 nm; (c) Optical graph of freestanding film 6FDA-PI, 70 μm.

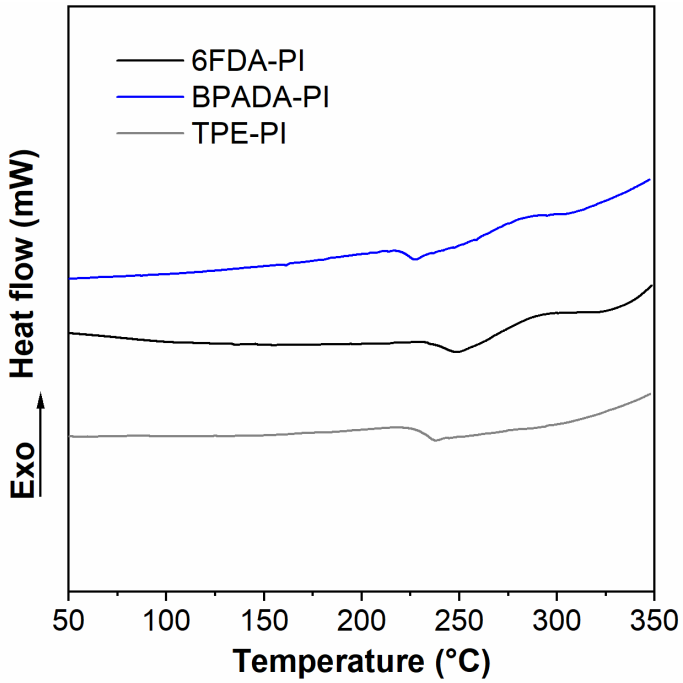

Supplementary Fig. 29. DSC curves of PIs.

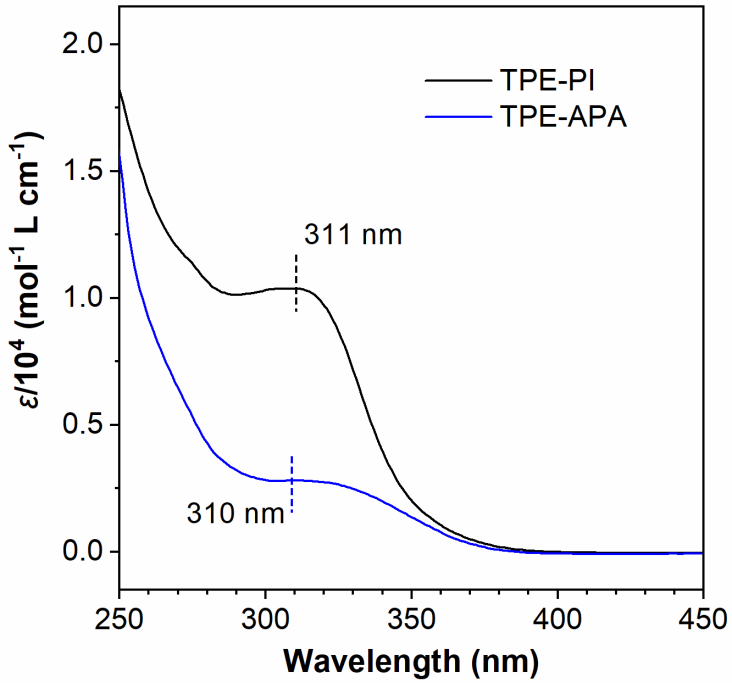

Supplementary Fig. 30. Absorption spectra of TPE-APA and TPE-PI in THF solutions. Solution concentration: 10 μM.

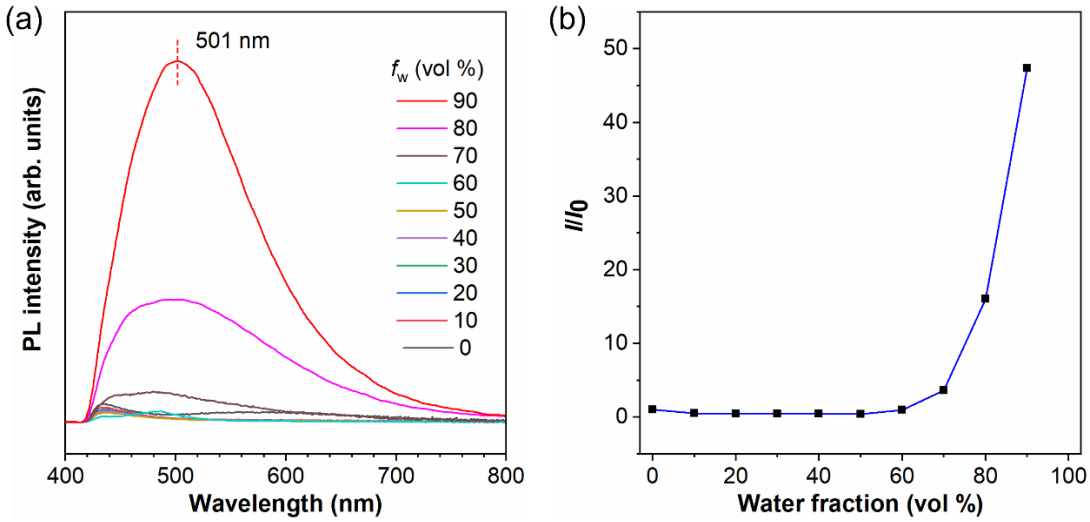

Supplementary Fig. 31. PL spectra. (a) PL spectra of TPE-APA in THF/water mixtures with different water fractions. Solution concentration: 10 μM. (b) Plot of relative emission intensity (I/I_0) versus the composition of the THF/water mixture of TPE-APA.

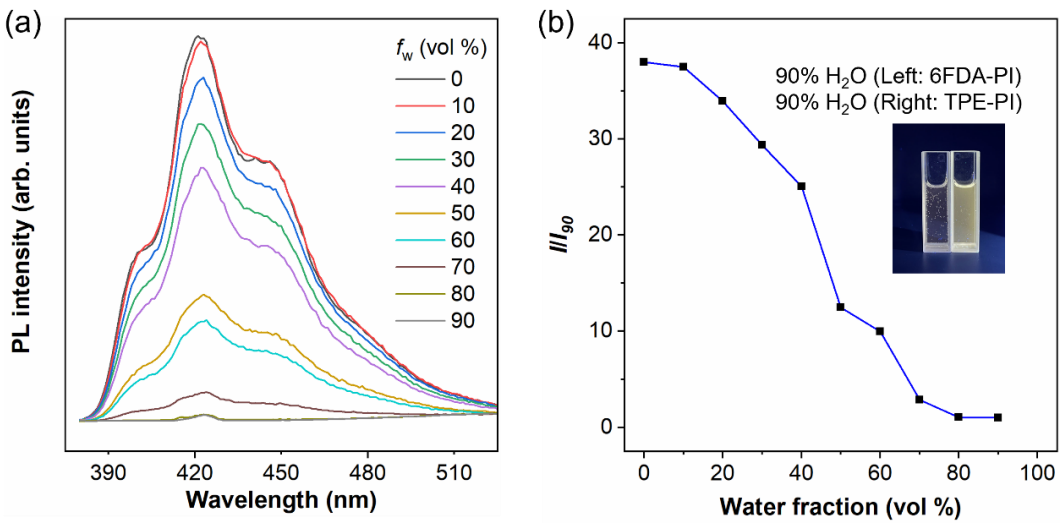

Supplementary Fig. 32. PL spectra. (a) PL spectra of 6FDA-PI in THF/water mixtures with different water fractions. Solution concentration: 100 μM. (b) Plot of relative emission intensity (I/I_{90}) versus the composition of the THF/water mixture of 6FDA-PI. Inset: the associated fluorescent photographs of 6FDA-PI and TPE-PI solutions with water fraction of 90%.

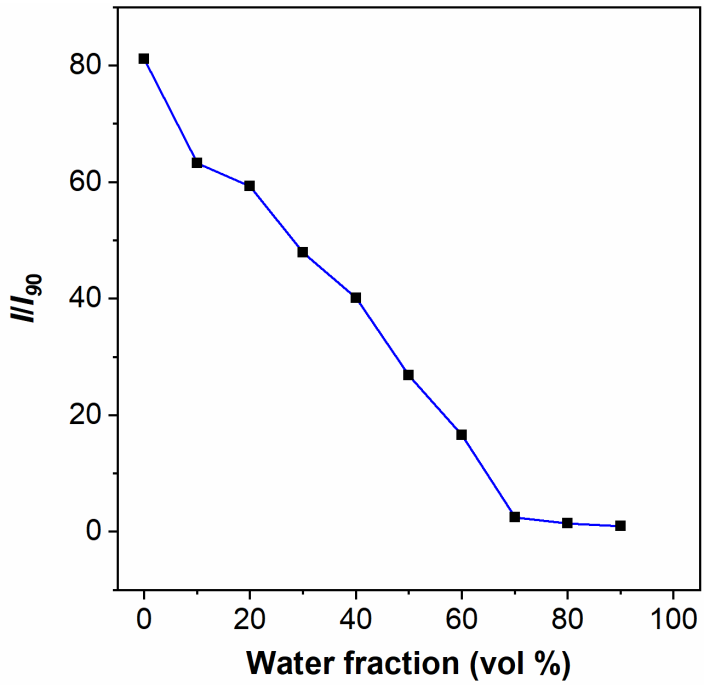

Supplementary Fig. 33. Plot of relative emission intensity (I/I_{90}) at 422 nm versus the composition of the THF/water mixture of TPE-PI.

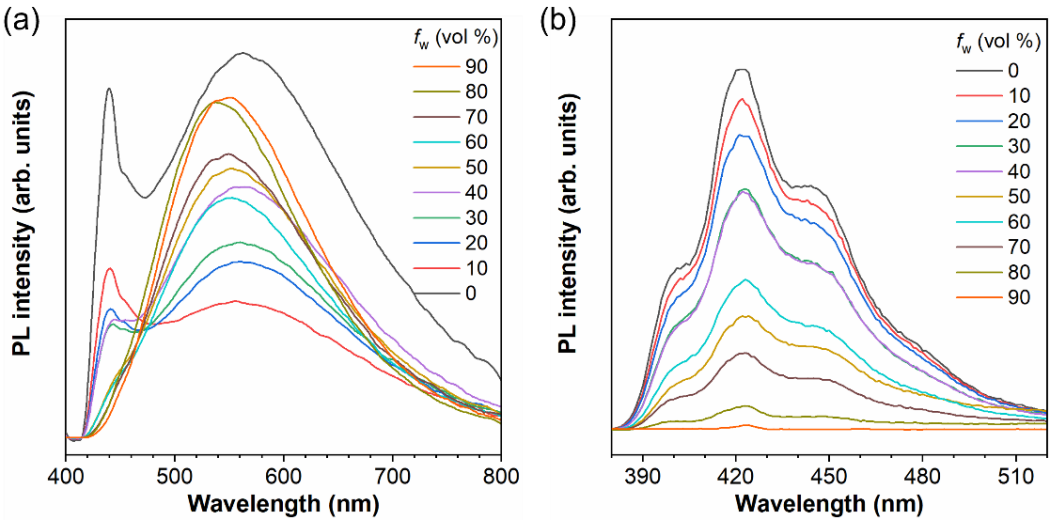

Supplementary Fig. 34. PL spectra. PL spectra of TPE-PI in THF/water mixtures with different water fractions. (a) Solution concentration: 1 mM; (b) Solution concentration: 10 μM.

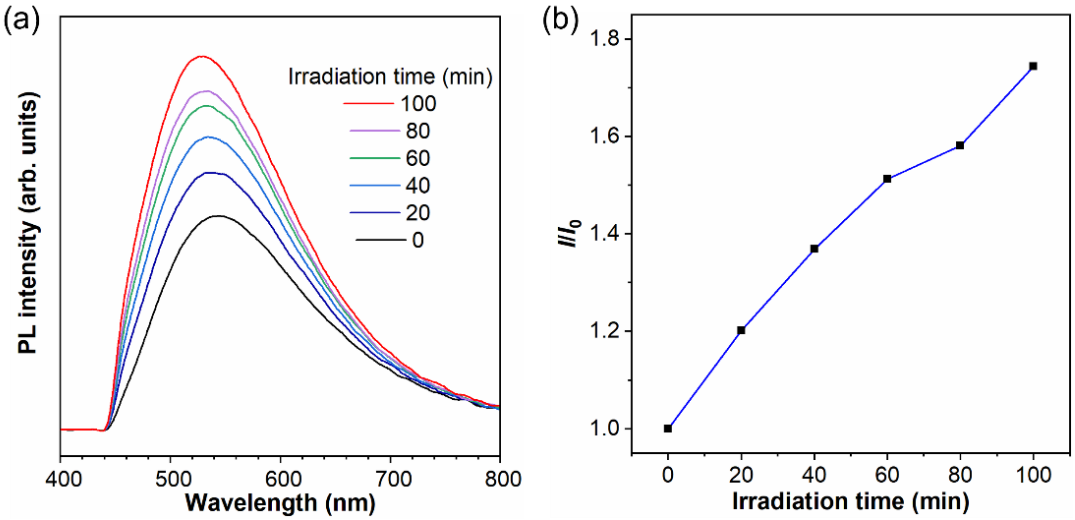

Supplementary Fig. 35. PL spectra. (a) PL spectra of the thin film of TPE-PI before and after UV irradiation with different time (light intensity was ~100 mW cm^{-2}), (b) Plot of relative emission intensity (I/I_0) versus irradiation time.

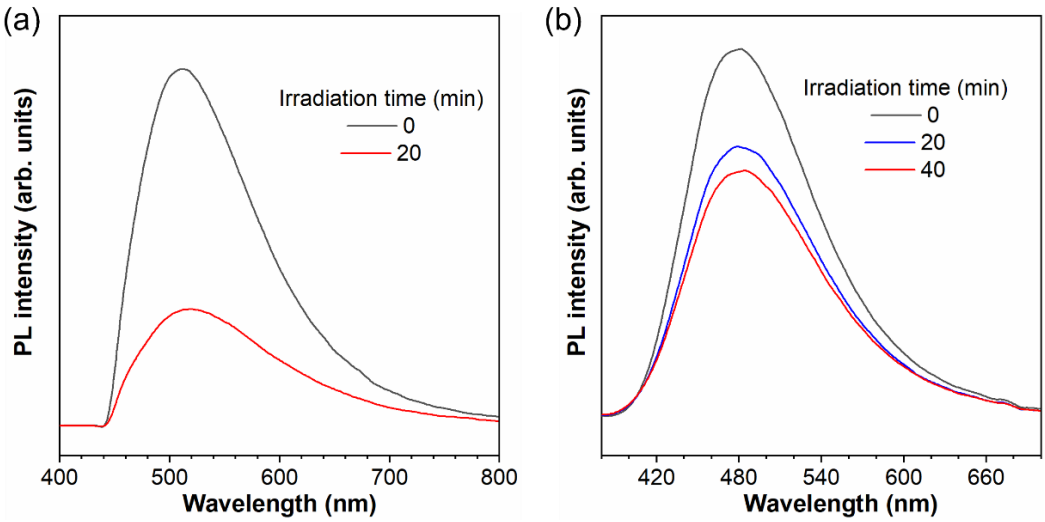

Supplementary Fig. 36. PL spectra. PL spectra of (a) thin film of monomer TPE-APA and (b) mixed film of monomer TPE-APA and PMMA before and after UV irradiation. (light intensity was ~100 mW cm^{-2})

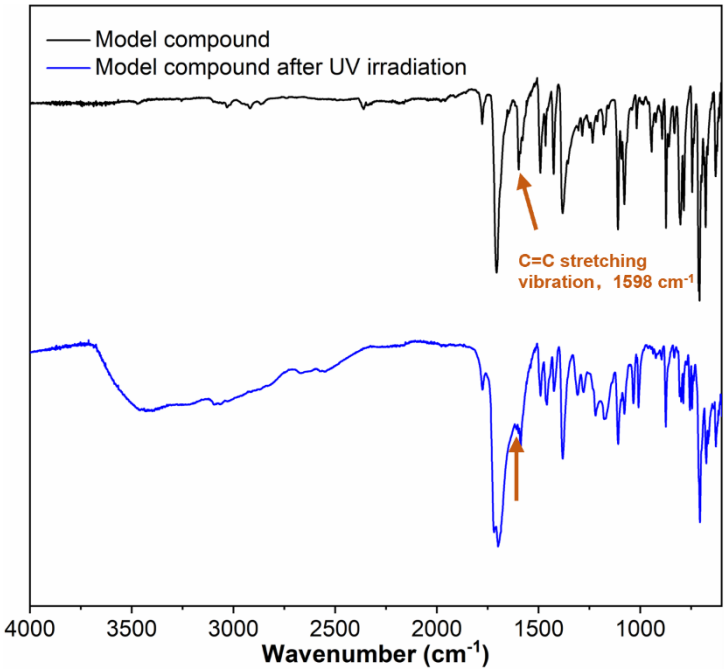

Supplementary Fig. 37. FT-IR spectra of the model compound before and after UV irradiation.

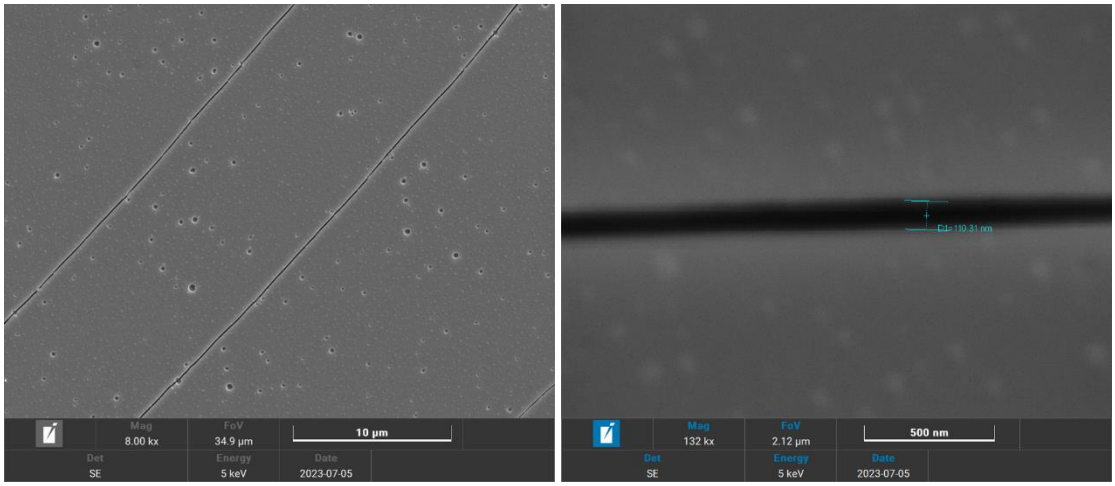

Supplementary Fig. 38. The microtraces of the front side of the 6FDA-PI film after UV irradiation.

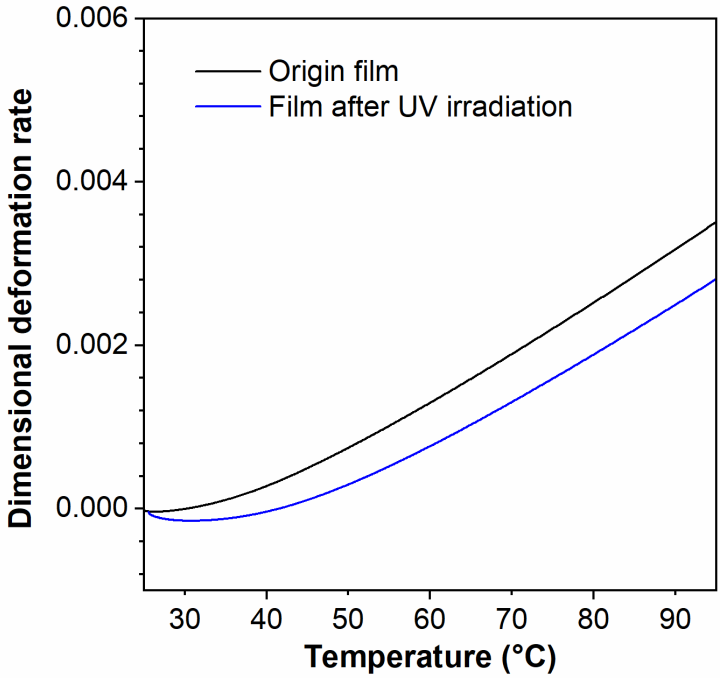

Supplementary Fig. 39. The thermal expansion curves of the 6FDA-PI films before and after UV irradiation.

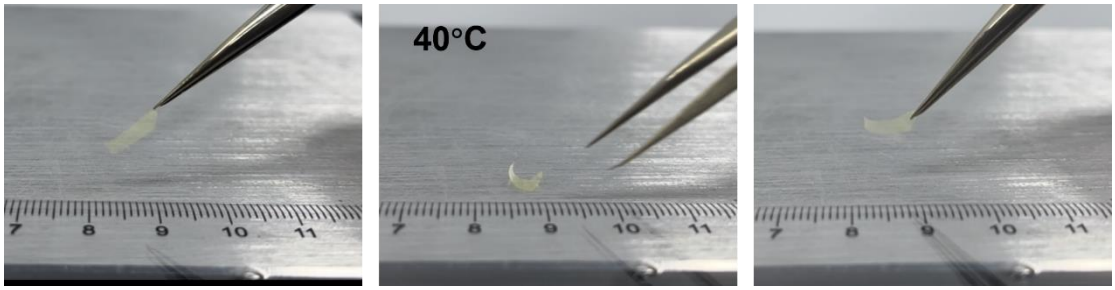

Supplementary Fig. 40. Actuation of the exposed 6FDA-PI film at 40 ° C heating table.

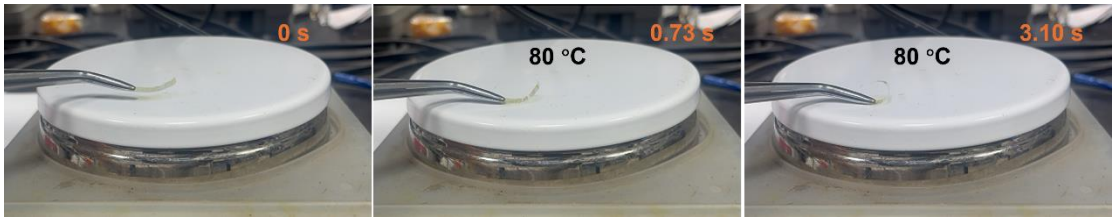

Supplementary Fig. 41. Actuation of the exposed 6FDA-PI film at 80 ° C heating table.

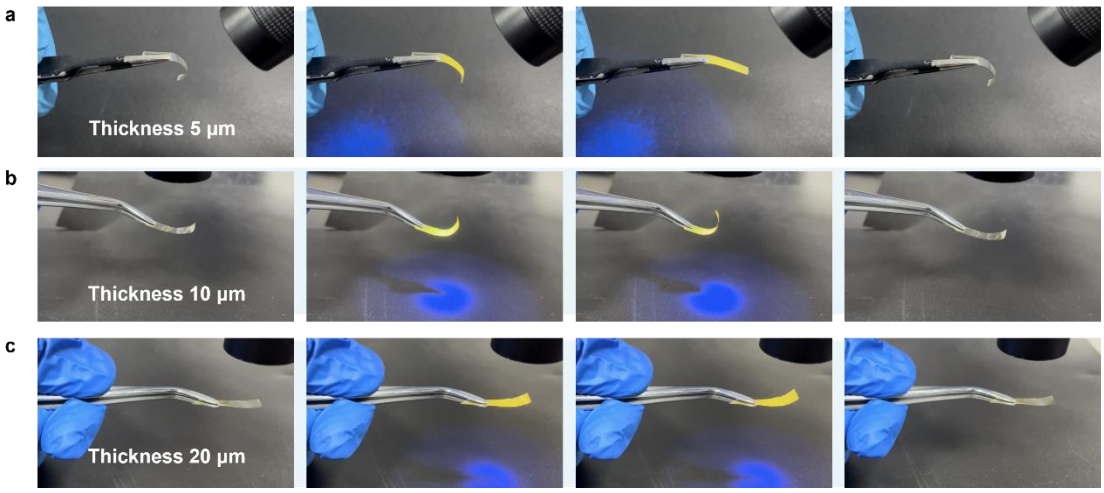

Supplementary Fig. 42. Photographs to show actuation of the exposed 6FDA-PI films with different thicknesses. (a) Actuation of the exposed 6FDA-PI film with a thickness of 5 μm. (b) Actuation of the exposed 6FDA-PI film with a thickness of 10 μm. (c) Actuation of the exposed 6FDA-PI film with a thickness of 20 μm.

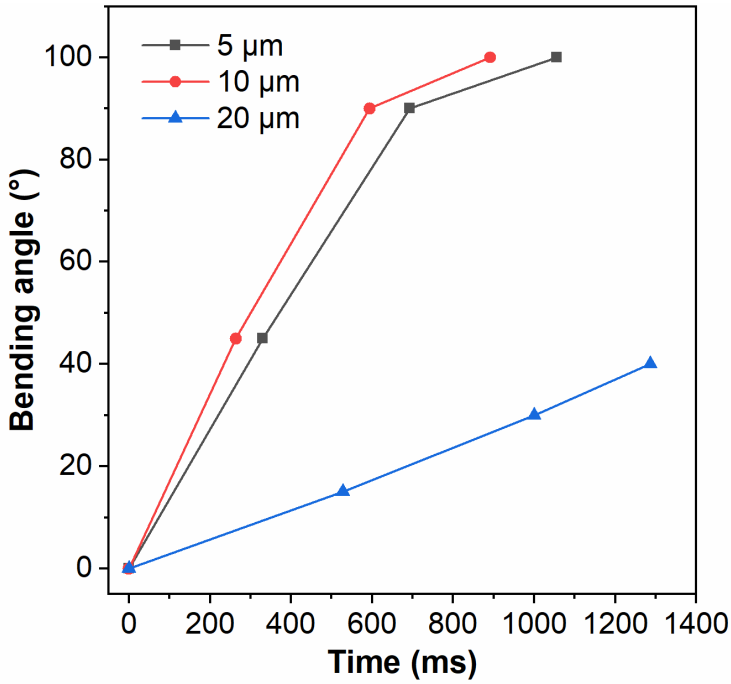

Supplementary Fig. 43. The bending angles of the exposed 6FDA-PI films with different thicknesses.

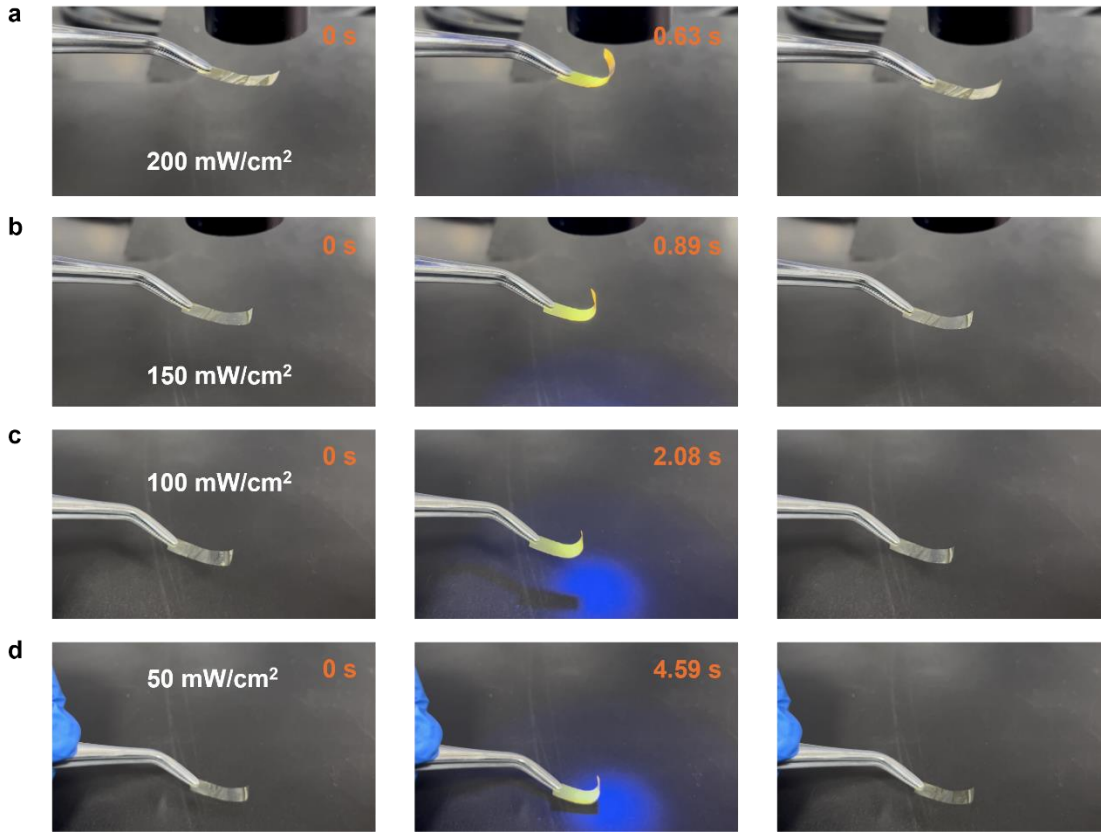

Supplementary Fig. 44. Photographs to show actuation of the exposed 6FDA-PI films under the UV exposion of different intensity. (a) Actuation of the exposed 6FDA-PI film with intensity of 200 mW/cm^2. (b) Actuation of the exposed 6FDA-PI film with intensity of 150 mW/cm^2. (c) Actuation of the exposed 6FDA-PI film with intensity of 100 mW/cm^2. (d) Actuation of the exposed 6FDA-PI film with intensity of 50 mW/cm^2.

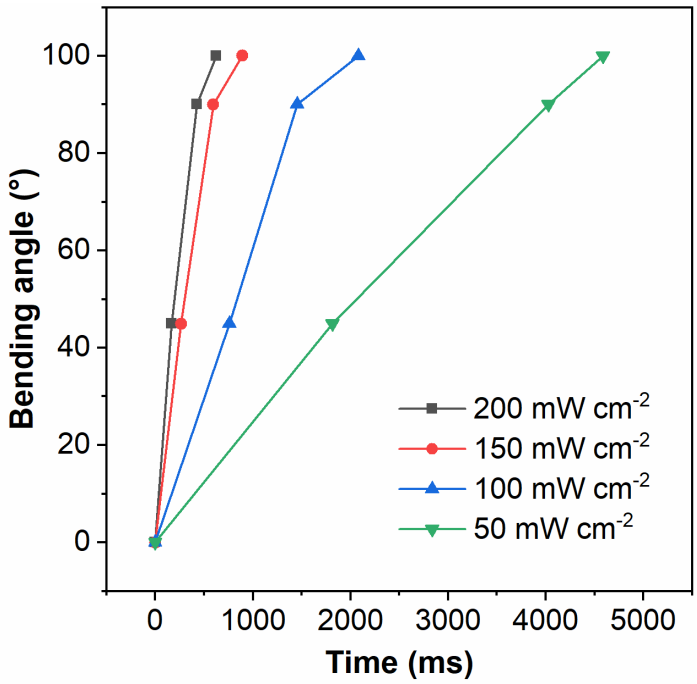

Supplementary Fig. 45. The bending angles of the exposed 6FDA-PI films under the UV exposion of different intensity.

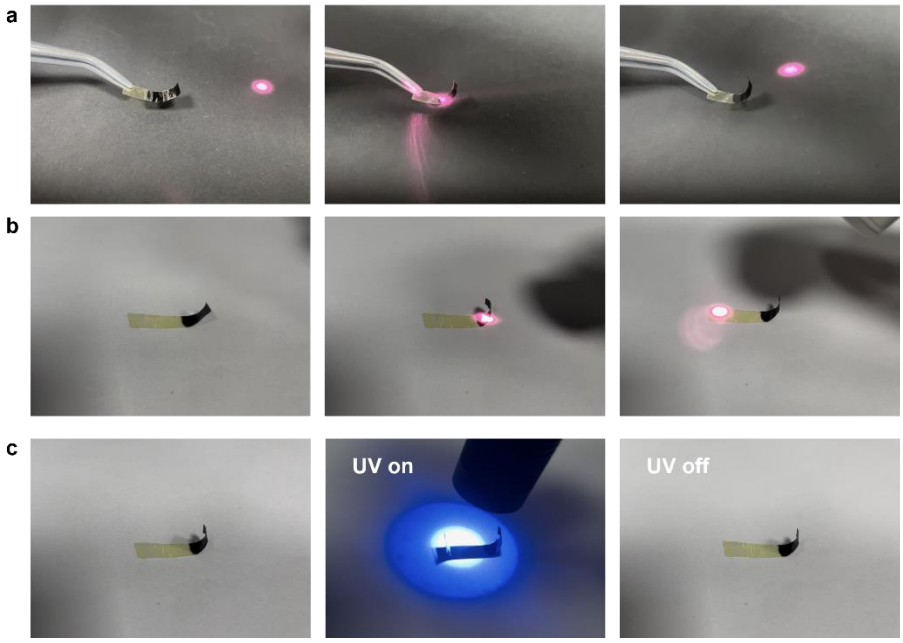

Supplementary Fig. 46. Actuation of the exposed 6FDA-PI film. (a) Actuation of the exposed 6FDA-PI film under 808 nm light. (b) Different actuation on both sides of the film. (c) Actuation of the exposed 6FDA-PI film under UV light.

IV. References

1. Worch, J. C., Stubbs, C. J., Price, M. J. & Dove, A. P. Click Nucleophilic Conjugate Additions to Activated Alkynes: Exploring Thiol-yne, Amino-yne, and Hydroxyl-yne Reactions from (Bio)Organic to Polymer Chemistry. *Chem. Rev.* **121**, 6744-6776 (2021).
2. Rekondo, A. et al. Catalyst-Free Room-Temperature Self-Healing Elastomers Based on Aromatic Disulfide Metathesis. *Mater. Horiz.* **1**, 237-240 (2014).
3. Martin, R. et al. The Processability of a Poly(Urea-Urethane) Elastomer Reversibly Crosslinked with Aromatic Disulfide Bridges. *J. Mater. Chem. A* **2**, 5710- 5715 (2014)